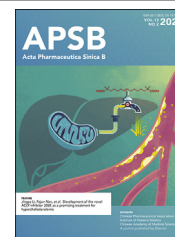




Chinese Pharmaceutical Association
Institute of Materia Medica, Chinese Academy of Medical Sciences

Acta Pharmaceutica Sinica B

www.elsevier.com/locate/apsb
www.sciencedirect.com



ORIGINAL ARTICLE

Nanopolyphenol rejuvenates microglial surveillance of multiple misfolded proteins through metabolic reprogramming



Dayuan Wang^a, Xiao Gu^a, Xinyi Ma^a, Jun Chen^b, Qizhi Zhang^b,
Zhihua Yu^a, Juan Li^a, Meng Hu^a, Xiaofang Tan^a, Yuyun Tang^a,
Jianrong Xu^{a,d}, Minjun Xu^b, Qingxiang Song^a, Huahua Song^a,
Gan Jiang^a, Zaiming Tang^c, Xiaoling Gao^{a,*}, Hongzhuan Chen^{a,d,*}

^aDepartment of Pharmacology and Chemical Biology, State Key Laboratory of Oncogenes and Related Genes, Shanghai Universities Collaborative Innovation Center for Translational Medicine, Shanghai Jiao Tong University School of Medicine, Shanghai 200025, China

^bKey Laboratory of Smart Drug Delivery, Ministry of Education, School of Pharmacy, Fudan University, Shanghai 201203, China

^cKey Laboratory of Cell Differentiation and Apoptosis of Chinese Ministry of Education, Shanghai Jiao Tong University School of Medicine, Shanghai 200025, China

^dShanghai Frontiers Science Center of TCM Chemical Biology, Institute of Interdisciplinary Integrative Medicine Research, Shanghai University of Traditional Chinese Medicine, Shanghai, 201203, China

Received 4 April 2022; received in revised form 14 June 2022; accepted 15 June 2022

KEY WORDS

Microglia;
Metabolism;
Misfolded proteins;
Phagocytosis;
Degradation;
Polyphenol;
Nanoparticles;
Neurodegenerative
diseases

Abstract Microglial surveillance plays an essential role in clearing misfolded proteins such as amyloid-beta, tau, and α -synuclein aggregates in neurodegenerative diseases. However, due to the complex structure and ambiguous pathogenic species of the misfolded proteins, a universal approach to remove the misfolded proteins remains unavailable. Here, we found that a polyphenol, α -mangostin, reprogrammed metabolism in the disease-associated microglia through shifting glycolysis to oxidative phosphorylation, which holistically rejuvenated microglial surveillance capacity to enhance microglial phagocytosis and autophagy-mediated degradation of multiple misfolded proteins. Nanoformulation of α -mangostin efficiently delivered α -mangostin to microglia, relieved the reactive status and rejuvenated the misfolded-proteins clearance capacity of microglia, which thus impressively relieved the neuropathological changes in both Alzheimer's disease and Parkinson's disease model mice. These findings provide

*Corresponding authors. Tel./fax: +86 21 63846590 776580, +86 21 64674721 (Xiaoling Gao).

E-mail addresses: shellygao1@sjtu.edu.cn (Xiaoling Gao), yaoli@shsmu.edu.cn (Hongzhuan Chen).

Peer review under responsibility of Chinese Pharmaceutical Association and Institute of Materia Medica, Chinese Academy of Medical Sciences.

<https://doi.org/10.1016/j.apsb.2022.07.014>

2211-3835 © 2023 Chinese Pharmaceutical Association and Institute of Materia Medica, Chinese Academy of Medical Sciences. Production and hosting by Elsevier B.V. This is an open access article under the CC BY-NC-ND license (<http://creativecommons.org/licenses/by-nc-nd/4.0/>).

direct evidences for the concept of rejuvenating microglial surveillance of multiple misfolded proteins through metabolic reprogramming, and demonstrate nanoformulated α -mangostin as a potential and universal therapy against neurodegenerative diseases.

© 2023 Chinese Pharmaceutical Association and Institute of Materia Medica, Chinese Academy of Medical Sciences. Production and hosting by Elsevier B.V. This is an open access article under the CC BY-NC-ND license (<http://creativecommons.org/licenses/by-nc-nd/4.0/>).

1. Introduction

Neurodegenerative disease includes Alzheimer's disease (AD) and Parkinson's disease (PD) has become a serious public health problem. However, effective disease-modifying approaches are still unavailable. The accumulation of misfolded proteins such as amyloid-beta plaque ($A\beta$) in AD, tau formed paired helical filaments (PHF) in AD, and α -synuclein preformed fibril (PFF) in PD is a common and key pathogenesis in neurodegenerative diseases^{1,2}. To reduce these misfolded proteins, potential therapeutics were designed to correct misfolding or target clearance using antibody or proteasome³, but due to the complex structure and ambiguous pathogenic species of the misfolded proteins, these methods still lack the efficiency to inhibit the formation or clear the key toxic species of the misfolded proteins³. Therefore, developing a universal approach to identify and clear the misfolded proteins despite their structures and species might provide a more feasible strategy to treat neurodegenerative diseases.

Microglia surveillance plays the key role in identifying and clearing misfolded proteins to maintain homeostasis in the brain⁴. But in neurodegenerative diseases, the chronic insults induce over-reaction and over production of reactive oxygen species (ROS) in microglia^{5,6}. The excessive ROS directly damages mitochondria and causes dysfunction of metabolism, while the damage of mitochondria releases more ROS and further damages other normal mitochondria, resulting in the aggravation of metabolic dysfunction. The sustained metabolic disorder ruins the innate surveillance function in microglia^{6,7}, which could cause and aggravate the protein misfolding^{5,8–10}. Accordingly, we here proposed that restoring metabolic balance may rejuvenate microglial surveillance function and provide a universal approach to clear the multiple misfolded proteins and treat various neurodegenerative diseases.

Natural polyphenols including resveratrol, quercetin and curcumin have been used to intervene in metabolism-associated diseases such as obesity and diabetes^{11,12}. Therefore, polyphenols might be potential metabolic-modulators for the dysfunctional microglia in neurodegeneration. Our previous study found that a polyphenol, α -mangostin (α -M), increased microglial clearance of $A\beta$ ¹³, but the underlying mechanism remained largely unknown. Accordingly, it was possible that α -M might rejuvenate microglial surveillance of misfolded proteins through metabolic modulation and serve as a universal therapy against neurodegenerative diseases.

To test the above hypothesis, we performed RNA-sequencing (RNAseq) analysis in microglia upon α -M treatment, and found that α -M reprogrammed metabolism in microglia. Further investigation showed that α -M reprogrammed metabolism in the misfolded protein-treated (disease-associated) microglia by inducing a shift from glycolysis to oxidative phosphorylation (OXPHOS) and restored the energy balance in the cell. We then disclosed that α -M reprogrammed the metabolism through activating AMP-

activated protein kinase (AMPK) and holistically enhanced the clearance of the misfolded proteins: α -M not only enhanced microglial phagocytosis of the misfolded proteins but also promoted autophagy-mediated degradation of the misfolded proteins in microglia. These effects relied on the activation of AMPK. To realize microglia-targeting delivery of α -M *in vivo*, we prepared α -M-encapsulated nanoparticle (NP- α -M) as described previously¹³. NP- α -M successfully functioned in microglia and promoted the clearance of $A\beta$, PHF and PFF, and rescued the neuropathological changes in AD and PD model mice. Collectively, our study introduces a novel way for clearing multiple misfolded proteins through microglial metabolic reprogramming, and demonstrates that NP- α -M might serve as a universal drug to treat various neurodegenerative diseases.

2. Materials and methods

2.1. Cell lines and cell cultures

BV-2 (3111C0001CCC000063) is an immortalized cell line that behaves the same function and morphology of microglia. Primary microglia were isolated from the cortex of the one-day postnatal mice as described previously¹⁴. DMEM with 10% fetal bovine serum, 1% penicillin streptomycin, 1% L-glutamine and 1% non-essential amino acids were used to culture the cells in the standardized environment (37 °C, 5% CO₂, 95% relative humidity).

2.2. Mice

3 × TG mice were from Jackson Laboratory (#34830-JAX). C57BL/6 mice were from Shanghai SLAC Laboratory Animal. All experimental procedures were approved by the Ethics Committee for Animal Experimentation of Shanghai Jiao Tong University School of Medicine. The mice were housed in the sterile cages equipped with laminar airflow hoods in a temperature constant room at 22–25 °C and provided with the circulation of 12 h light and 12 h dark. All mice were fed with autoclaved chow and water.

2.3. Preparation and characterization of NP- α -M

NP- α -M was prepared through emulsion/solvent evaporation as described previously¹³. Briefly, 0.5 mg α -M and 10 mg PEG-PLA were dissolved in 1 mL dichloromethane. Afterward, 2 mL 1% aqueous sodium cholate (*w/v*) was added. Probe sonication (220 w) was then given to the mixture to produce an O/W emulsion. Next, 18 mL 0.5% aqueous sodium cholate (*w/v*) was added into the emulsion and a magnetic stirrer system was used to homogenize the mixture. Rotary evaporator (Shanghai Institute of Organic Chemistry, ZX-98, Shanghai, China) was then used to evaporate dichloromethane in the mixture. The nanoparticles were

collected through centrifugation at $14,000 \times g$ (Thermo Fisher, Multifuge X1R, Waltham, Massachusetts, USA) for 45 min. At last, a $1.5 \text{ cm} \times 20 \text{ cm}$ sepharose CL-4B column was used to remove the untrapped α -M. Coumarin-6 was used to label the nanoparticles *via* a similar procedure.

The zeta potential and particle size of NP- α -M were measured using a Zetasizer detector (Nano-ZS, Malvern, UK). The drug loading capacity and encapsulation efficiency were measured ($n = 3$) using high performance liquid chromatography (HPLC) and calculated as described previously¹⁵.

2.4. Preparation of PFF and PHF

PFF was prepared as described previously¹⁶. Briefly, 5 mg/mL recombinant α -synuclein proteins (NKMAX, SNA2001L, Seongnam-si, Korea) in phosphate buffer saline (PBS) was stirred with a magnetic stirrer at 1000 rpm, 37 °C (IKA, 0025004975, Wilmington, North Carolina, USA). It took one-week incubation to form the aggregates, then diluted the aggregates to 0.1 mg/mL with PBS. At last, using a sonifier to sonicate (0.5 s pulse on/off) the aggregates for 30 s at 10% amplitude. PFF was validated using TEM and stored at -80 °C before use. PHF was prepared as described previously^{17–19}. Briefly, recombinant tau protein (Rockland, 009-001-T86S, Philadelphia, Pennsylvania, USA) in 2.5 mmol/L D,L-dithiothreitol, 100 mmol/L NaCl and 10 mmol/L HEPES, pH 7.4 was incubated with heparin at a molar protein:heparin ratio of 4:1. Constant orbital agitation at 1000 rpm, 37 °C (IKA) was required for 72 h. The remaining free heparin should be removed by filter-centrifugation. PHF was validated using TEM and stored at -80 °C before use.

2.5. Preparation of the diseased-associated microglia and drug treatment

The disease-associated microglia were obtained by incubating microglia with PFF (3.6 $\mu\text{g/mL}$) or PHF (1 $\mu\text{g/mL}$) for 1 h. For drug treatment, as both phagocytosis and degradation of PFF/PHF were relatively fast^{20,21}, PFF/PHF was added after α -M/NP- α -M treatment, which can mimic the effect of α -M/NP- α -M on microglial clearance of the newly generated misfolded proteins *in vivo*. Specifically, microglial cells were treated with vehicle or α -M (400 ng/mL) or NP- α -M (containing 400 ng/mL α -M) for 24 h, and at the last 1 h of the treatment, PFF (3.6 $\mu\text{g/mL}$) or PHF (1 $\mu\text{g/mL}$) was added in the medium and incubated for 1 h.

2.6. Mice treatment

PD mouse model was established as described previously¹⁶, and with a few changes. Briefly, three-month-old C57BL/6 mice were anesthetized with xylazine and ketamine, and a microinjector was stereotaxically and unilaterally inserted into the striatum of the right hemisphere at the following coordinates: 0.2 mm anteroposterior; 2.0 mm from bregma, mediolateral; 2.6 mm dorsoventral. 2 μL of 2.5 $\mu\text{g}/\mu\text{L}$ PFF in PBS with the infusion rate of 0.2 $\mu\text{L}/\text{min}$ was injected. Mice received the same operation procedure without the injection of PFF were used as the Sham group.

$3 \times$ TG mice were intravenously injected with NP- α -M (1 mg/kg α -M), α -M (1 mg/kg), NP (37.5 mg/kg, the same NP dose as that of in the NP- α -M) or 0.9% saline per day for one month. PD model mice were treated the same way as that of the $3 \times$ TG mice at the time of one month after PFF injection, and the Sham-operated mice

were treated with 0.9% saline. Female and male mice were equally distributed in each group.

2.7. Behavioral tests

Open-field test (OFT). OFT was carried out as described previously²², and with a few changes. Briefly, the mice were placed in a box (30 cm \times 30 cm \times 15 cm) for 5 min. The motion path and time were recorded.

Y-maze test. The test was carried out as described previously²², and with a few changes. Briefly, there are three horizontal arms (arm 1, arm 2, arm 3, 40 cm long, 3 cm wide, 12 cm high of each) in the Y-maze. The mice were placed in arm 1 and the entry sequence *e.g.*, 123132 (the numbers were arm codes) and the entry times of each arm were recorded over a 5 min period.

Object recognition test (ORT). ORT was carried out as described previously²². Briefly, one day before the experiment, the mice were habituated in the open-field apparatus for 10 min without any object. Short-term memory evaluation: two identical objects A and A' were placed in the apparatus, and either object was 10 cm far from the wall. The mice were placed to the opposite side of the objects close to the wall and trained for 5 min as the first training phase. 90 min after, in the second 5 min training phase, object A' was replaced by object B with different color and shape. Long-term memory evaluation: 24 h after the second training phase, object B was replaced by object C which was different in color and shape from other objects. The mice were placed into the apparatus and trained for 5 min. The recognition index was [the exploration time of the novel object/(the exploration time of the familiar object + the exploration time of the novel object)%].

Morris water maze test was carried out as described previously²³, and with a few changes. Briefly, one day ahead of the experiment, the mice were habituated in the water maze (120 cm in diameter). The maze was filled with black water which was maintained at 18 °C–22 °C. The maze was divided into four quadrants, and a platform (10 cm in diameter) was fixed 1 cm beneath the surface of the water. In the training, the mice were allowed to swim freely and search for the platform for 1 min. If the mice can't find the platform successfully, they will be guided to it and allowed to stay on it for 30 s. Each mouse was trained four times a day from four different quadrants with different sequences and the presented data are the average of the four trials. The escape latency and swimming path were recorded by a tracking system (Shanghai Jiliang Software Technology, Shanghai, China). On the sixth day, the platform was removed and the mice were placed in the opposite quadrant of the previous platform quadrant. Each mouse was trained two times and the presented data are the average of the two trials. The swimming path and time were recorded.

Rotarod test. The test was carried out as described previously¹⁶. Briefly, the time that the mice remained on the accelerating rotarod cylinder (Ugo basile, 47750, Gemonio, Italy) was measured. The speed of the cylinder started from 4 rpm and slowly accelerated to 40 rpm in 5 min. The time count ended if the mice fell down on the plastic plates or gripped the rungs without trying to walk again on the device for two consecutive revolutions. Three trials were recorded and the mean duration was calculated. The mice were pre-trained for two days before the actual test day.

Pole test. The test was carried out as described previously¹⁶. Briefly, a metal rod with a length of 75 cm and a diameter of 9 mm

wrapped with bandage gauze was used for the mice to grab. First, the mice were first acclimatized in the operation room for 30 min before the test. Then, the mice were put at 7.5 cm from the top of the pole and the heads should be facing upwards. The total time that the mice took from the start position to the base of the pole was recorded. The longest recording time was 60 s.

2.8. Safety assessment

The safety of NP- α -M were evaluated after intravenously injection per day for one month. The blood was sampled with the serum collected for biochemical analysis. Total protein, albumin, total bilirubin, triglyceride, cholesterol, alanine aminotransferase, and aspartate aminotransferase were used as the indicators of liver function, and urinary acid, creatine kinase, creatinine, and urea indices in the serum were applied as the indicators of renal function. As previously documented, hematoxylin and eosin (HE) staining was used to examine the morphology of the heart, liver, spleen, lung, and kidney²⁴.

2.9. Immunohistochemistry

The immunohistochemical staining of TH²⁵, A β ¹³, PHF²⁶, and IBA-1¹³ were performed as previously described. The following antibodies were used: rabbit monoclonal anti-tyrosine hydroxylase (Abcam, ab137869, Cambridge, UK), mouse monoclonal anti-A β (6E10) (SIG-39320, Covance, Burlington, North Carolina, USA); mouse monoclonal anti-phospho-Tau (Ser202, Thr205) (AT8) (Thermo Fisher, MN1020, Waltham, Massachusetts, USA).

2.10. Western blot analysis

Brain tissue lysates were prepared as described previously¹⁶. For cell lysates, the cells were homogenized in radio-immunoprecipitation assay (RIPA) buffer with 10 mmol/L PMSF and 1 mmol/L EDTA. The homogenate was centrifuged at 14,000 rcf for 15 min. After that, the supernatants were collected, and the protein concentration was measured using bicinchoninic acid (BCA) assay kit (Thermo Fisher, 23227). Fifty micrograms of protein were used in the immunoblot analysis. Western blot procedure was performed as described previously¹³. The following primary antibodies were used: rabbit monoclonal anti-tyrosine hydroxylase (Abcam, ab137869), rabbit monoclonal anti-alpha-synuclein (Abcam, ab212184), rabbit monoclonal anti-phospho-alpha-synuclein (Ser129) (Abcam, ab51253), mouse monoclonal anti- β -actin (Beyotime Biotechnology, AA128, Shanghai, China), mouse monoclonal anti-GAPDH (Beyotime Biotechnology, AF0006), mouse monoclonal anti-LC3B (Cell Signaling Technology, 83506S, Danvers, Massachusetts, USA), rabbit monoclonal anti-AMPK α (5831S, Cell Signaling Technology), rabbit monoclonal anti-phospho-AMPK α (Thr172) (Cell Signaling Technology, 2535S), rabbit monoclonal anti-LKB1 (Cell Signaling Technology, 3047S), rabbit monoclonal anti-phospho-LKB1 (Ser428) (Cell Signaling Technology, 3482S), rabbit monoclonal anti-PGC-1 α (Cell Signaling Technology, 2178S), rabbit monoclonal anti-mTOR (Cell Signaling Technology, 2983S), rabbit monoclonal anti-phospho-mTOR (Ser2448) (Cell Signaling Technology, 5536S), rabbit monoclonal anti-SQSTM1/P62 (Cell Signaling Technology, 39749).

2.11. Confocal microscopy

Cells were seeded on glass-bottom-96-well plates which pre-coated with poly-L-lysine at a density of 5×10^3 cells per well. After treatments as described above. The cells were rinsed by PBS and incubated over night at 4 °C with the primary antibody diluted in 10% goat serum and 0.5% Triton in PBS. The cells were then washed twice and stained with the secondary antibodies for 1 h at room temperature. DAPI (Beyotime Biotechnology, C1006) was used to stain the nuclei at room temperature for 10 min. A laser scanning confocal microscope (Leica, TCS SP8, Wetzlar, Germany) was used to acquire the images.

The following primary antibodies were used: mouse monoclonal anti-phospho-Tau (Ser202, Thr205) (AT8) (Thermo Fisher, MN1020), rabbit monoclonal anti-alpha-synuclein (Abcam, ab138501), rabbit monoclonal anti-IBA1 (Abcam, ab178847), rabbit monoclonal anti-Tom20 (Cell Signaling Technology, 42406S), mouse monoclonal anti-LC3B (Cell Signaling Technology, 83506S).

The following secondary antibodies were used: goat anti-rabbit secondary antibody, Alexa Fluor plus 488 (Thermo Fisher, A32731), goat anti-mouse secondary antibody, Alexa Fluor 488 (Thermo Fisher, A32723), goat anti-rabbit secondary antibody, Alexa Fluor plus 647 (Thermo Fisher, A32733).

2.12. Transmission electron microscopy

Microglia samples were processed as described previously²⁷, and the tissue samples were processed as described previously²⁸. The ultrathin sections were obtained using ultramicrotome (LEICA, EM UC7, Wetzlar, Germany) and observed using a transmission electron microscope (HITACHI, H-67650, Tokyo, Japan).

2.13. ELISA analysis

The tissues were homogenized, and the proteins were extracted and diluted using Cell Extraction Buffer PTR for assay. The cell culture supernatant was centrifuged at 2000 g (Thermo Fisher) for 10 min to remove the debris and diluted using Sample Diluent NS, and then collected for assay. The cells were rinsed twice and incubated in Cell Extraction Buffer PTR on ice for 20 min and centrifuged at $18000 \times g$ (Thermo Fisher) for 20 min, and then the supernatants were collected and diluted using Cell Extraction Buffer PTR for assay. The misfolded proteins in the medium or cells were quantified using tau ELISA Kit (Abcam, ab273617) or alpha-synuclein ELISA Kit (Abcam, ab260052). TNF- α , IL-1 β , and IL-6 in the brain tissues were quantified using TNF alpha ELISA Kit (Abcam, ab208348), IL-1 β ELISA Kit (Abcam, ab197742), or IL-6 ELISA Kit (Abcam, ab222503). The experimental procedures were performed according to the manufacturer's instructions.

2.14. Cell transfection

Lipofectamine™ 3000 Transfection Reagent (Thermo Fisher, L3000075) was used for plasmid cell transfections following the manufacturer's instructions. The transfection procedure was performed as described previously²⁹.

2.15. Microglia isolation in the brain

The isolation of microglia in the brain parenchyma was performed as described previously³⁰. Briefly, the mice were anesthetized and perfused with PBS buffer. The brain was extracted

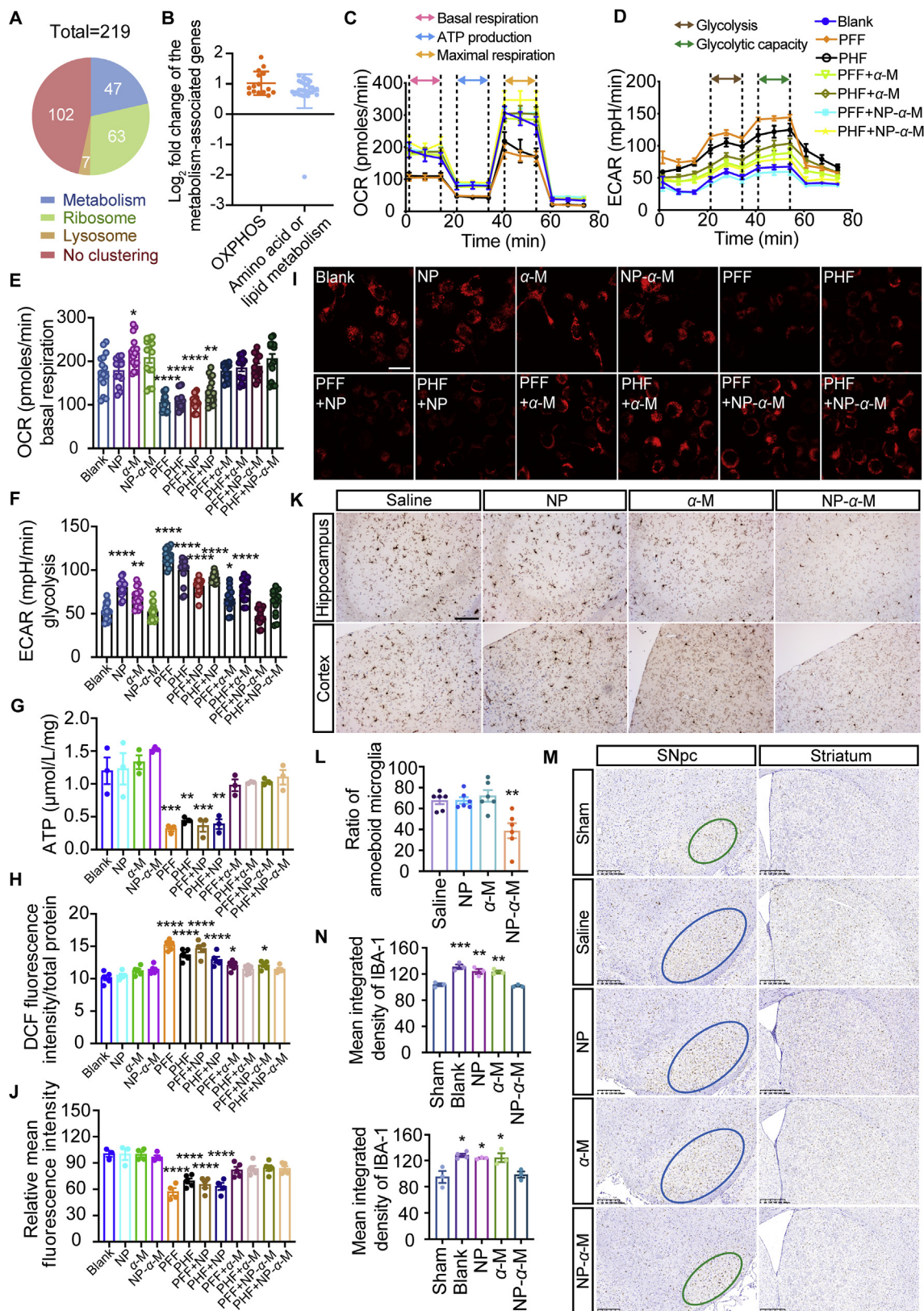


Figure 1 NP- α -M reprograms metabolism and relieves reactive state in the disease-associated microglia. (A) Pathway clustering of the 219 significantly changed ($P \leq 0.05$) genes upon 400 ng/mL α -M treatment (compared with control group); (B) Log₂ fold change of the OXPHOS (15 genes) and amino acid and lipid metabolism (31 genes) among the 47 significantly changed metabolic genes in (A); (C to F), OCR and ECOR measurements in microglia under the treatments as indicated (PFF, 3.6 μ g/mL; PHF, 1 μ g/mL; α -M or α -M in NP- α -M, 400 ng/mL) ($n = 5$); (G) Total ATP production in microglia under different treatments as indicated ($n = 3$). The ATP concentration was normalized to the protein

and the hypothalamus was dissociated. The single cell suspension was prepared using a neural dissociation kit (Miltenyi Biotech, 130-092-628, Bergisch Gladbach, North Rhine-Westphalia, Germany), and then centrifuged at $700 \times g$ (Thermo Fisher) for 15 min in a continuous 30% Percoll gradient. Next, the cells were incubated with biotin-conjugated anti-CD11b antibody (Thermo Fisher, 13-0112-82), and CD11b positive cells were then isolated by Dynabeads Biotin Binder (Thermo Fisher, 11047).

2.16. Q-TOF LC-MS

To extract α -M in the brain parenchyma, the brain tissue was ultrasonic homogenized in deionized water, and then flutamide (internal standard) methanol solution was added and vortex for 1 min. Then, the homogenate was centrifuged at 10,000 rpm for 10 min (Thermo Fisher). The supernatant was used to determine α -M concentration in the brain parenchyma. To extract α -M in the isolated microglia from the brain, microglia were first centrifuged to remove the supernatant, and then flutamide methanol solution was added to the microglia and vortex for 1 min. Then, the homogenate was centrifuged at 10,000 rpm for 10 min (Thermo Fisher). The supernatant was used to determine α -M concentration in microglia. The LC-QTOF-MS (Agilent, 6545, Santa Clara, California, USA) was used to detect α -M. The chromatography was performed using the Venusil XBP Phenyl analytical column (Agilent, 2.1 mm \times 100 mm, 5.0 μ m). The detecting procedure was performed as described previously¹³. Briefly, the mobile phase contained 0.5% formic acid solution (A) and 99.5% methanol (B), the flow rate was set at 0.4 mL/min, and using the negative-ion mode. The gradient was set from 45% to 5% A in the first 3 min, and held for 2.5 min, and then returned to 45% A from 5.6 to 7 min. The voltage of the needle was set at 4.5 kV, the temperature was 600 °C. The pressure of GS1 nebulizer gas (nitrogen) was set at 50 psi, GS2 turbo heater gas was 50 psi, curtain gas (nitrogen) was 10 psi, and collision gas (CAD, nitrogen) in the collision cell was 12 psi. The collision energy for α -M was -41 V, and for flutamide was -34 V, the declustering potential was -100 V, and the entrance potential was -10 V. The multiple reaction monitoring (MRM) mode was used to detect the ions, and the detecting parameter for α -M was m/z 409.2/351.1 and for flutamide was 274.9/201.9.

The concentration of α -M in microglia was calculated by the amount of α -M in microglia (ng)/the total protein in microglia (mg). The concentration of α -M in brain parenchyma was calculated by the amount of α -M in the brain parenchyma (ng)/the total protein in the brain parenchyma (mg).

2.17. Measurement of ATP level

The ATP level was measured using the ATP Assay Kit (Beyotime Biotechnology, #S0026) according to the manufacturer's instruction. Briefly, removed the culture medium in the plate, and added the lysis buffer (1/10 volume of the culture medium), then centrifuged at 2000 g (Thermo Fisher) for 5 min and the supernatant was collected. Before detecting the supernatant, the ATP detecting buffer was pre-added into the plate and incubated for 5 min at room temperature to minimize the background signal. Next, added the supernatant into the ATP detecting buffer, mixed, and incubated for 5 min at room temperature. After that, the luminescence was measured, and the ATP level was normalized to the protein concentration.

2.18. Measurement of ROS level

The ROS level was measured using the ROS Assay Kit (Beyotime Biotechnology, #S0033S) according to the manufacturer's instruction. Briefly, the DCFH-DA (10 mmol/L) was diluted using DMEM (1:1000). The culture medium was replaced by DCFH-DA (10 μ mol/L), and incubated at 37 °C for 20 min. After that, the cells were rinsed using DMEM for three times, and then the fluorescence signal was measured, and the ROS level was normalized to the protein concentration in microglia.

2.19. Seahorse extracellular flux test

The OCR and ECOR measurements were performed using the XF Cell Mito Stress Test Kit (Agilent, #103015-100) and XF Glycolysis Stress Test Kit (Agilent, #103020-100) according to the manufacturer's instruction, and measured using a Seahorse XFe 96 Extracellular Flux Analyzer (Seahorse Bioscience, North Billerica, Massachusetts). Briefly, 2×10^4 /well microglia were seeded into the Seahorse XF 96-well culture plate overnight, and then treated with the drugs as indicated. The assay medium and the solution of the modulators were prepared as instructions. The modulators include oligomycin, carbonyl cyanide-4 (trifluoromethoxy) phenylhydrazone (FCCP), and rotenone-antimycin (Rot/AA) are for OCR measurement, and glucose, oligomycin, and 2-deoxy-glucose (2-DG) are for ECOR measurement. The final concentration of oligomycin was 1.5 μ mol/L, FCCP was 1 μ mol/L, and other modulators were prepared as instructions. The cells were rinsed twice using the assay medium, and the working solution of the modulators was loaded into the ports on sensor cartridge. After that, the plate was loaded into the analyzer to run the assay. During the assay, the modulators were

concentration in microglia; (H) DCF fluorescence intensity in microglia measured by Reactive Oxygen Species Assay Kit ($n = 5$). The fluorescence intensity was normalized to the protein concentration in microglia; (I) Representative images of mitochondrion (TOM-20) staining in microglia under different treatments as indicated. Scale bar, 20 μ m; (J) Quantification of TOM-20 fluorescence intensity using ImageJ software ($n = 3-5$). The fluorescence intensity was relative to the Blank group; (K) Representative images of IBA-1 staining in the cortex and hippocampus from the $3 \times$ TG mice. Scale bar, 120 μ m. 10-month-old $3 \times$ TG mice were intravenously injected with 0.9% saline, NP (the same NP dose as that of in the NP- α -M), α -M (1 mg/kg) or NP- α -M (α -M, 1 mg/kg) per day for one month; (L) Quantification of the number of amoeboid microglia in the cortex and hippocampus from the $3 \times$ TG mice ($n = 6$ from three mice per group); (M) Representative images of IBA-1 staining in the SNpc and striatum from the PD model mice. The green circles represented normal microglial proliferations, while the blue circles represented the enhanced microglial proliferations. The size of the circle represented the extend of the proliferation area. Scale bar, 300 μ m. The treatment of the PD model mice was the same as that of the $3 \times$ TG mice, besides, sham-operated mice were treated with 0.9% saline. (N) Quantification of the mean integrated intensity of IBA-1 in the SNpc (above) and striatum (below) from the PD model mice using ImageJ software ($n = 3$ mice per group). Data are means \pm SEM. * $P < 0.05$, ** $P < 0.01$, *** $P < 0.001$, **** $P < 0.0001$ significantly different with that of the Blank (E, F, G, H and J) or Saline (L) or Sham (N) group. One-way ANOVA, followed by Tukey's multiple comparisons test.

sequentially injected into the well from the ports, and the oxygen consumption rate (OCR) and extracellular acidification rate (ECOR) were measured.

2.20. Statistical analysis

All the statistical analyses were performed by Prism (GraphPad, 8, San Diego, California, USA). All data in this article were shown as mean \pm SEM. Student's *t* test or one-way ANOVA followed by Tukey's multiple comparisons test was used to assess the significance in group comparisons. Differences with $P < 0.05$ were considered statistically significant and the significant levels were indicated as * $P < 0.05$, ** $P < 0.01$, *** $P < 0.001$, **** $P < 0.0001$.

3. Results

3.1. α -M/NP- α -M reprogrammed metabolism and protect the disease-associated microglia

To explore the potentiality of α -M in promoting microglial surveillance of misfolded proteins through metabolic modifications, we performed RNAseq and found that upon α -M treatment, 219 genes significantly changed ($P \leq 0.05$, fragments per kilobase of exon model per million mapped fragments (FPKM) ≥ 50 and \log_2 Fold change >0.59 or < -1 , compared with control group), among which 47 genes (21.5%) associated with cellular metabolism, 63 genes (28.8%) clustered in ribosome and 7 genes (3.2%) clustered in lysosome (Fig. 1A). These results indicated that α -M significantly regulated metabolism in microglia. Among the 47 changed metabolic genes, 16 genes were found related to glucose metabolism in which 15 genes associated with OXPHOS (all up-regulated), 31 metabolic genes were found associated with amino acid or lipid metabolism with 30 genes up-regulated and only 1 gene down-regulated (Fig. 1B). These metabolic genes are involved in the metabolism of various nutrients, suggesting that α -M reprogrammed the metabolism in microglia, but among which OXPHOS in glucose metabolism was particularly enhanced.

Though α -M reprogrammed metabolism in microglia, the low bioavailability limited its further application *in vivo*. To overcome such limitation, we prepared NP- α -M as described previously¹³. The characterization of NP- α -M was shown in Supplementary Table 1, the stability of NP- α -M was shown in Supporting Information Fig. S1, the drug release of NP- α -M and the pharmacokinetics and biodistribution of α -M and NP- α -M had been characterized in our previous study¹³. Upon NP- α -M treatment, 129 genes significantly changed, among which 33 genes (25.58%) associated with cellular metabolism. In these metabolic changed genes, 14 genes related to OXPHOS and all up-regulated (Figs. S2A and S2B). These results were very similar with that of upon α -M treatment, suggesting that NP- α -M reprogrammed metabolism as efficiently as α -M.

Microglia suffer from a metabolic failure caused by a switch from OXPHOS to anaerobic glycolysis in neurodegenerative diseases⁶. As RNAseq indicated that α -M/NP- α -M enhanced OXPHOS in microglia, we presumed that α -M/NP- α -M might be metabolically protective in microglia in neurodegeneration. To test this hypothesis, we treated microglia with misfolded proteins to simulate the aggregation abundant environment like that of in the neurodegenerative diseases. The misfolded protein-treated microglia were defined as disease-associated microglia. Then,

we performed Seahorse tests to measure glucose metabolism in microglia, finding that the misfolded proteins switched the metabolism from OXPHOS to anaerobic glycolysis and decreased ATP production in microglia, but α -M/NP- α -M reversed the metabolic phenotype from glycolysis back to OXPHOS (Fig. 1C–F and Figs. S2C–E) and recovered efficient ATP production in microglia (Fig. 1G).

Most ATP is produced from OXPHOS in mitochondria³¹, and ROS is a main destructor of mitochondria in microglia in neurodegeneration^{6,32}. We found that misfolded proteins exacerbated ROS production in microglia, but largely reversed by α -M/NP- α -M (Fig. 1H). We also evaluated the state of mitochondria using TOM-20 antibody, and found that the misfolded proteins decreased the expression of TOM-20 in microglia, but restored by α -M/NP- α -M (Fig. 1I and J), suggesting that α -M/NP- α -M ameliorated the damage of mitochondria in the disease-associated microglia. Such mitochondrial protective effect of α -M was also verified *in vivo* in the $3 \times$ TG mice (a widely used AD mouse model with aggregated A β and tau pathology) through transmission electron microscope (TEM) analysis, which showed that NP- α -M ameliorated the damage of mitochondria in glial cells (Fig. S2F). Metabolic status is closely related to microglial activation⁶, and the metabolic protective effect of α -M also attenuated the overactivation of microglia in neurodegeneration. As shown in immunohistochemistry (IHC) tests, 67.55% IBA-1 positive microglia were amoeboid microglia in the cortex and CA2 hippocampus of the saline-treated $3 \times$ TG mice, but decreased to 38.71% following the treatment of NP- α -M (Fig. 1K and L). Similarly, in PD model mice, compared with saline, NP- α -M treatment decreased the proliferation of IBA-1 positive microglia by 22.43% in the substantia nigra pars compacta (SNpc) and 23.07% in the striatum (Fig. 1M and N).

3.2. α -M/NP- α -M switched the metabolic phenotype through activating AMPK in the disease-associated microglia

To explore how α -M/NP- α -M switched the metabolic phenotype in the disease-associated microglia, we focused on AMPK due to the similar consequences of AMPK activation in metabolic regulation³³. The total AMPK expression did not change upon any treatment (Fig. 2A and B). But threonine172 (Thr172) phosphorylation of the α -subunit in AMPK (p-AMPK) decreased when treated with misfolded proteins, and restored upon α -M/NP- α -M treatment (Fig. 2A and C). To further verify the metabolic modulation was activated by AMPK, we detected the upstream and downstream molecules of AMPK when regulates metabolism, such as liver kinase B1 (LKB1) and peroxisome proliferator-activated receptor gamma coactivator 1-alpha (PGC-1 α). Western blot showed that total LKB1 did not change upon treatments (Fig. 2D and E). But the phosphorylation of LKB1 at Ser428 decreased after misfolded proteins treatment, and restored upon α -M/NP- α -M treatment (Fig. 2D and F). Misfolded proteins also down-regulated PGC-1 α expression in microglia, but α -M/NP- α -M restored it (Supporting Information Fig. S3A and B). These results indicated that misfolded proteins damaged AMPK-associated pathway, but α -M/NP- α -M restored it. Moreover, we used a classic AMPK inhibitor, compound C, to block AMPK activation. The inhibition of AMPK activation by compound C was verified by Western blot (Fig. 2G–I). Upon compound C treatment, α -M/NP- α -M failed to convert the metabolic phenotype from anaerobic glycolysis to OXPHOS in the misfolded proteins-treated microglia, and compound C alone did not affect

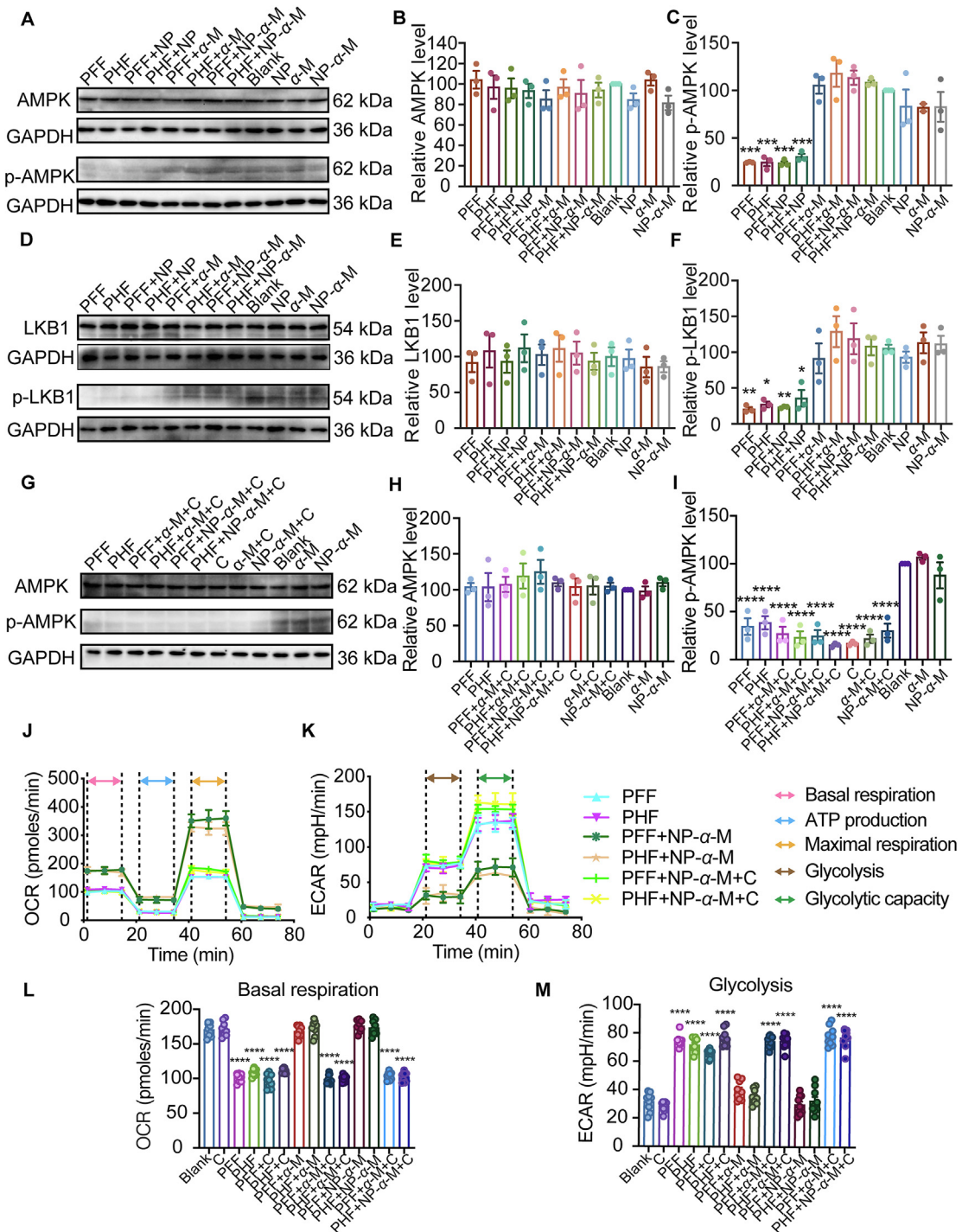


Figure 2 NP-α-M induces the metabolic shift through activating AMPK in the disease-associated microglia. (A to C) AMPK and p-AMPK were extracted from BV2 cells treated as indicated (PFF, 3.6 μg/mL; PHF, 1 μg/mL; α-M or α-M in NP-α-M, 400 ng/mL; NP, the same concentration as that of in NP-α-M), and examined by Western blot. The Lines' intensity was quantified using ImageJ software ($n = 3$); (D to F) LKB1 and p-LKB1 were extracted from BV2 cells treated as indicated, and examined by Western blot. The Lines' intensity was quantified using ImageJ software ($n = 3$); (G to I) AMPK and p-AMPK were extracted from BV2 cells treated as indicated (Compound C, C, 10 μmol/L), and examined by Western blot. The Lines' intensity was quantified using ImageJ software ($n = 3$); (J to M) OCR and ECOR measurements in microglia under the treatments as indicated ($n = 3$). Expression level was relative to the Blank (B, C, E, F, H, I) group. Data are means ± SEM. * $P < 0.05$, ** $P < 0.01$, *** $P < 0.001$, **** $P < 0.0001$ significantly different with that of the Blank (B, C, E, F, H, I, L and M) group. One-way ANOVA, followed by Tukey's multiple comparisons test.

the metabolism in microglia (Fig. 2J–M, and Figs. S3C–E). These results indicated that α -M/NP- α -M switched the metabolic phenotype to rescue the energy deficiency by activating AMPK in the disease-associated microglia.

3.3. α -M/NP- α -M rejuvenated phagocytosis of the misfolded proteins in the disease-associated microglia

Microglial surveillance clears misfolded proteins through phagocytosis and degradation. To investigate whether the restoration of metabolic balance could ameliorate the surveillance function in the disease-associated microglia, we first evaluated microglial phagocytosis of the misfolded proteins. BV2 cells were treated with vehicle or α -M (400 ng/mL) or NP- α -M (containing 400 ng/mL α -M) for 24 h, and at the last 1 h of the treatment, PFF (3.6 μ g/mL) or PHF (1 μ g/mL) was added in the medium and incubated for 1 h (Supporting Information Fig. S4A). Immunofluorescence (IF) analysis showed that, compared with vehicle, microglia treated with α -M/NP- α -M internalized more misfolded proteins (Fig. 3A and B). To further quantify the amount of misfolded proteins phagocytosis, the same treatment as previously described was performed and enzyme-linked immunosorbent assay (ELISA) was used to detect intracellular (C1) and medium (M) level of PFF or PHF, and the uptake rate was calculated by $C1/(M+C1)$ %. We found that the uptake of misfolded proteins after α -M/NP- α -M treatment in microglia was about 20%–60% higher than that of in the vehicle treated microglia (Fig. 3C). We also performed the same phagocytosis test in primary microglia and got a similar outcome (Figs. S4B–E). These results indicated that α -M/NP- α -M enhanced misfolded proteins phagocytosis in microglia.

As α -M/NP- α -M restored the metabolic balance in the disease-associated microglia and microglial phagocytosis is an energy-intensive process^{6,34}, we therefore investigated whether the metabolic restoration could promote the phagocytosis of the misfolded proteins in the disease-associated microglia. In order to restrain the metabolic shift mediated by α -M/NP- α -M, we blocked AMPK activation using compound C before α -M/NP- α -M treatment. Next, we measured microglial phagocytosis using ELISA and found that blocking AMPK activation inhibited α -M/NP- α -M promoting the phagocytosis of the misfolded proteins in microglia (Fig. 3D). These results indicated that α -M/NP- α -M rejuvenated microglial phagocytosis of the misfolded proteins through AMPK-activated metabolic restoration.

3.4. α -M/NP- α -M rejuvenated degradation of the misfolded proteins in the disease-associated microglia

To measure microglial degradation of the misfolded proteins, BV2 cells were treated as mentioned above, but at the time point of 24 h, the misfolded proteins were removed in order to stop phagocytosis, and then continued to incubate microglia for 1 h (Supporting Information Fig. S4F). In this way, the change of intracellular misfolded proteins level (C2) in the last 1 h will mainly be the degradation amount. C2 was measured using ELISA, and the degradation rate was calculated by $(C1-C2)/C1$ %. The results showed that the degradation of misfolded proteins after α -M/NP- α -M treatment in microglia was approximately 20%–70% higher than that of in the vehicle treated microglia (Fig. 3E), indicating that α -M/NP- α -M enhanced misfolded proteins degradation in microglia. We also performed the same degradation test in primary microglia and got a similar outcome

(Figs. S4G and H). These results demonstrated that α -M/NP- α -M enhanced the degradation of misfolded proteins in microglia.

Next, we also blocked AMPK activation before α -M/NP- α -M treatment and measured degradation of the misfolded proteins using ELISA. The results showed that blocking AMPK activation inhibited α -M/NP- α -M promoting the degradation of the misfolded proteins in microglia (Fig. 3F), indicating that AMPK was also essential for promoting microglial degradation of the misfolded proteins.

As degradation does not require as much energy as phagocytosis³⁵, we then further investigated why metabolic restoration mediated by α -M/NP- α -M also enhanced degradation in microglia. Autophagy is an energy-producing process³⁶, and is also a main way to degrade phagocytosed-particles in microglia³⁷, so it is possible that α -M/NP- α -M restored the metabolic balance through autophagy while autophagy increased the degradation of the misfolded proteins. Accordingly, we evaluated autophagy activity in microglia upon α -M/NP- α -M treatment. We found that LC3 expression in α -M/NP- α -M treated BV2 cells was one-fold more than vehicle (Fig. 4A). We also transfected green fluorescent protein (Gfp) tagged Lc3 cDNA (Gfp-Lc3) into BV2 cells, and found that α -M/NP- α -M increased GFP puncta (Fig. 4B). Chloroquine (CQ) was used to further evaluate autophagy flux and we found that CQ and NP- α -M treated microglia expressed more LC3-II than single NP- α -M treatment (Fig. 4C). Autophagy promotion was also verified using multiple methods, such as detecting P62 (SQSTM1) expression, red fluorescent protein (RFP)-GFP-tandem tagged LC3 expression, and TEM, and found decreased P62 expression (Supporting Information Fig. S5A), increased RFP fluorescence (Fig. 4D), and increased autophagic vacuoles (Fig. S5B) upon α -M/NP- α -M treatment, respectively. Besides, in the $3 \times$ TG mice, confocal microscopy and Western blot both showed that NP- α -M increased the expression of total LC3 and microglial LC3 in the cortex and hippocampus (Supporting Information Fig. S6). In the PD model mice, NP- α -M also increased the expression of total LC3 and microglial LC3 in the striatum and SNpc (Supporting Information Fig. S7). These results collectively illustrated that α -M/NP- α -M enhanced autophagy in macroglia. Next, we used antibodies to indicate LC3 and misfolded proteins and confocal microscopy showed that in the presence of α -M/NP- α -M, most internalized misfolded proteins were surrounded by LC3 in microglia (Fig. 4E and F), indicating that the phagocytosed misfolded proteins were related to the autophagic components. As autophagy is a major way to degrade misfolded proteins in microglia, these results proved that the enhanced autophagy was involved in the promotion of misfolded proteins' degradation upon α -M/NP- α -M treatment. Like AMPK, mammalian target of rapamycin (mTOR) plays an important role in regulating metabolism and connects with AMPK³⁸, but it also acts as a crucial regulator in autophagy³⁹. So, we presumed that AMPK might associate with mTOR to enhance autophagy and thus promoted microglial degradation. To verify this hypothesis, we first measured p-mTOR and total mTOR expression in microglia and found that single misfolded proteins treatment did not change p-mTOR or mTOR level (Fig. 5A–C). But α -M/NP- α -M treatment down-regulated p-mTOR expression while total mTOR remained unchanged (Fig. 5A–C). To test whether AMPK regulated mTOR, we blocked AMPK activation using compound C, and found that α -M/NP- α -M failed to decrease p-mTOR in the disease-associated microglia (Fig. 5A and C). But compound C did not stop the decrease of p-mTOR induced by α -M/NP- α -M when the misfolded proteins were absence (Supporting Information

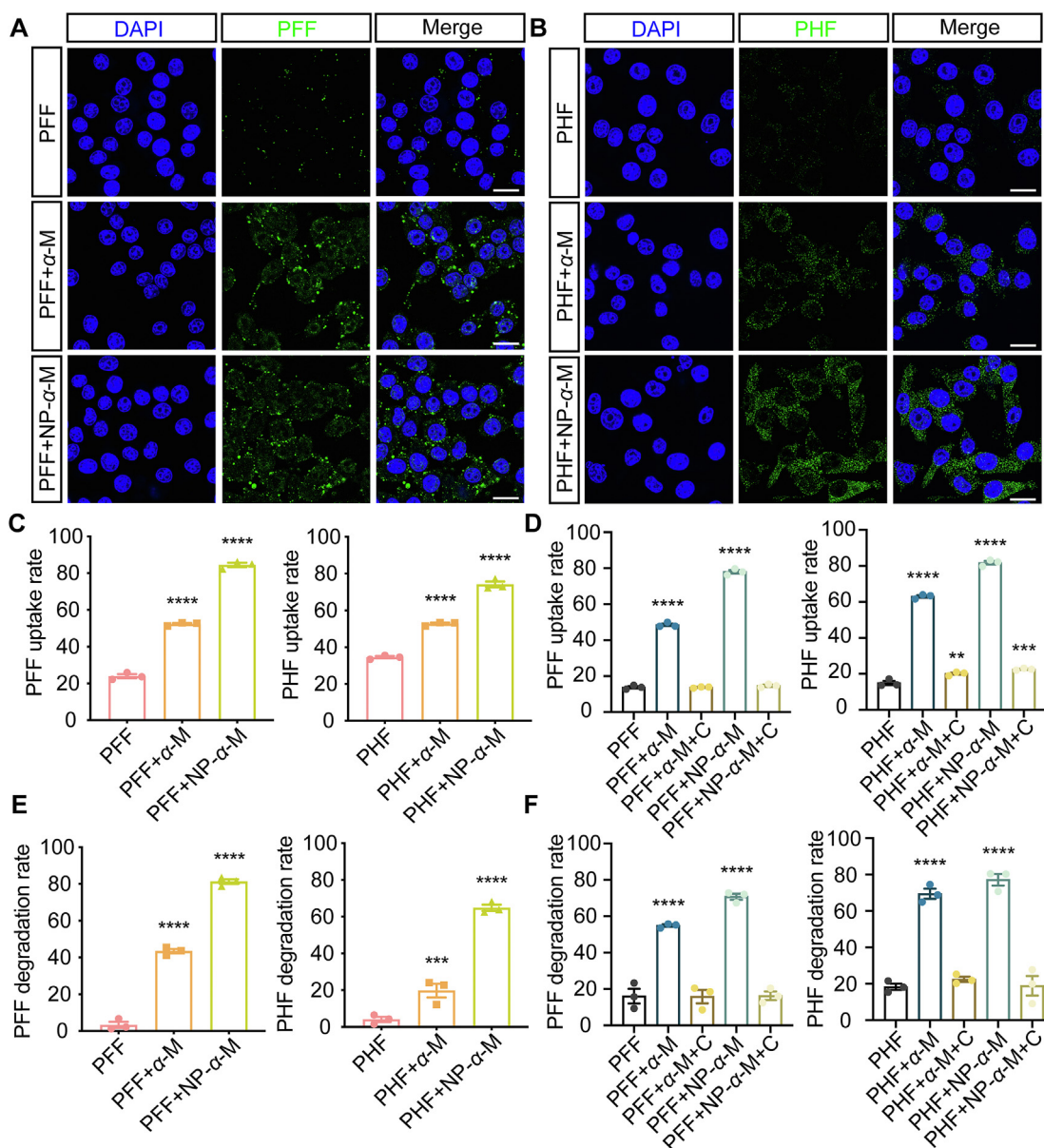


Figure 3 NP- α -M rejuvenates microglial clearance of the misfolded proteins through activating AMPK. (A and B) Representative images of PFF (α -synuclein) (A), and PHF (AT8) (B) staining in BV2 cells under different treatments as indicated (PFF, 3.6 μ g/mL; PHF, 1 μ g/mL; α -M or α -M in NP- α -M, 400 ng/mL). Scale bar, 20 μ m; (C and D) The levels of phagocytosis of the misfolded proteins (PFF or PHF) in microglia after α -M or NP- α -M treatment were measured using ELISA kits ($n = 3$), and the uptake rate was calculated. C, Compound C (10 μ mol/L) treatment before α -M or NP- α -M; (E and F) The levels of degradation of the misfolded proteins (PFF or PHF) in microglia after α -M or NP- α -M treatment were measured using ELISA kits ($n = 3$), and the degradation rate was calculated. Data are means \pm SEM. ** $P < 0.01$, *** $P < 0.001$, **** $P < 0.0001$ significantly different with that of the Blank (C and E) or PFF (D and F) group. One-way ANOVA, followed by Tukey's multiple comparisons test.

Figs. S8A and C). These results indicated that in the disease-associated microglia, α -M/NP- α -M inhibited mTOR required AMPK activation. Then, we measured LC3-II in microglia and found that α -M/NP- α -M failed to increase LC3-II in the disease-associated microglia when AMPK was inhibited (Fig. 5A and D). But AMPK inhibition did not stop the increase of LC3-II induced by α -M/NP- α -M when the misfolded proteins were absence (Figs. S8A and D).

These results collectively indicated that α -M/NP- α -M enhanced autophagy for restoring metabolic balance which also rejuvenated microglial degradation of the misfolded proteins.

3.5. NP- α -M promoted A β and PHF clearance and relieved neuropathological changes in AD model mice

α -M/NP- α -M holistically rejuvenated microglial surveillance of the misfolded proteins and attenuated overactivation in microglia, which might largely relieve the misfolded protein pathology and neuropathology in neurodegenerative diseases. To test this hypothesis, we first evaluated the safety of α -M/NP- α -M treatment at this dose *in vivo*, and found that neither α -M nor NP- α -M induce organ toxicity in the model mice (Supporting Information Figure S9). Then, we traced the distribution of NP- α -M in the

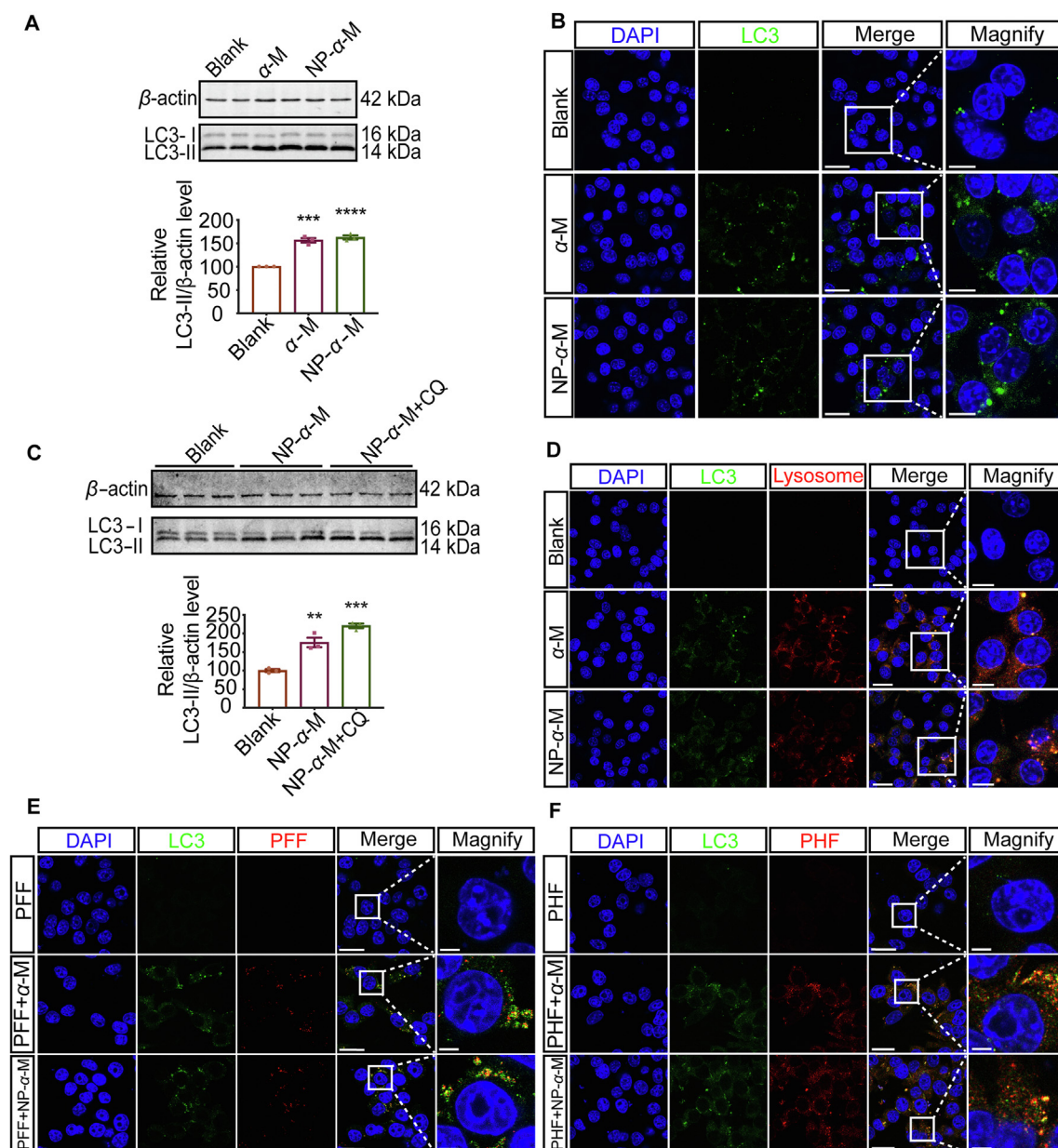


Figure 4 NP- α -M enhances autophagy which involves in the degradation of the misfolded proteins in microglia. (A) LC3-II was extracted from BV2 cells treated as indicated (α -M or α -M in NP- α -M, 400 ng/mL), and examined by Western blot. The Lines' intensity was quantified using ImageJ software ($n = 3$); (B) Representative images of the fluorescence of GFP-tagged LC3 in microglia under different treatments as indicated. Scale bar, 25 μ m. Zoom-in areas were enlarged from the boxes, scale bar, 10 μ m; (C) LC3-II was extracted from BV2 cells treated as indicated (Chloroquine, CQ, 20 nmoL/L), and examined by Western blot. The Lines' intensity was quantified using ImageJ software ($n = 3$); (D) Representative images of RFP-GFP-tandem-tagged LC3 in microglia under different treatments as indicated. Scale bar, 25 μ m. Zoom-in areas were enlarged from the boxes, scale bar, 10 μ m; (E and F) Representative images of LC3 (LC3B) and PFF (α -synuclein) (E) or LC3 (LC3B) and PHF (AT8) (F) costaining in microglia under different treatments as indicated (PFF, 3.6 μ g/mL; PHF, 1 μ g/mL). Scale bar, 25 μ m. Zoom-in areas were enlarged from the boxes, scale bar, 5 μ m. Expression level was relative to the Blank (A and C) group. Data are means \pm SEM. *** $P < 0.01$, **** $P < 0.0001$ significantly different with that of the Blank (A and C) group. One-way ANOVA, followed by Tukey's multiple comparisons test.

brain, Coumarin-6-labeled NP- α -M (Cou6-NP- α -M) was prepared and intravenously injected into 3 \times TG mice, 3 \times TG-wide-type (WT) mice (the same age as the 3 \times TG mice) at the dose of 1 mg/kg α -M per day for 7 days. After that, the mice were sacrificed to make brain slices and immunostained with anti-IBA-1 antibody. Confocal microscopy showed that Cou6-NP- α -M were substantially internalized by IBA-1 positive microglia in both

3 \times TG mice and 3 \times TG-WT mice (Supporting Information Fig. S10A), indicating that NP- α -M were effectively absorbed in microglia through intravenous injection *in vivo*. To further quantify the exact amount of α -M in microglia, 3 \times TG mice and C57BL/6 mice (the same age as the C57BL/6 PD model mice) were intravenously injected with NP- α -M at the dose of 1 mg/kg α -M per day for 7 days. After that, we isolated

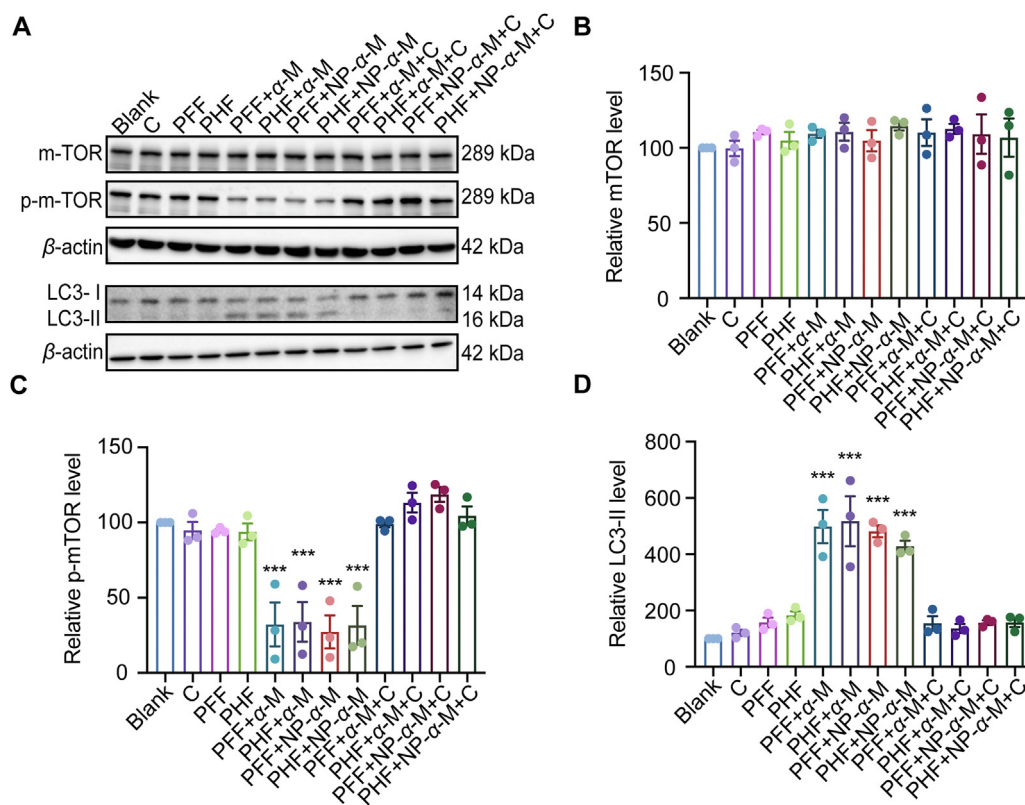


Figure 5 NP- α -M activates AMPK to inhibit mTOR and enhances autophagy in the disease-associated microglia. (A to D) mTOR, p-mTOR and LC3-II were extracted from BV2 cells treated as indicated (PFF, 3.6 μ g/mL; PHF, 1 μ g/mL; α -M or α -M in NP- α -M, 400 ng/mL; C, Compound C, 10 μ mol/L), and examined by Western blot. The Lines' intensity was quantified using ImageJ software ($n = 3$). Expression level was relative to the Blank (B, C and D) group. Data are means \pm SEM. *** $P < 0.001$ significantly different with that of the Blank (B, C and D) group. One-way ANOVA, followed by Tukey's multiple comparisons test.

microglia from a half brain, and detected α -M in the isolated microglia or α -M in brain parenchyma from the other half brain using quadrupole time of flight liquid chromatography mass spectrometer (Q-TOF LC-MS). We found that the average concentration of α -M in microglia among the $3 \times$ TG mice was 16.76 ng per mg tissue protein, and that was 2.9-fold higher than that of in the brain parenchyma, which was 5.82 ng per mg tissue protein (Fig. S10B); the average concentration of α -M in microglia among the C57BL/6 mice was 17.39 ng per mg tissue protein, and that was 3.2-fold higher than that of in the brain parenchyma, which was 5.36 ng per mg tissue protein (Fig. S10B). These results indicated that NP- α -M effectively and adequately accumulated in microglia *in vivo*, thus making microglia a valid function target of α -M.

Next, we measured the pathological changes in the AD model mice upon NP- α -M treatment. Apart from A β , PHF is another important pathogenic misfolded protein and hallmark in AD², so we investigated whether PHF was affected by NP- α -M in the AD model mice. NP- α -M was intravenously injected into $3 \times$ TG mice at the dose of 1 mg/kg α -M per day for one month. Besides, NP (37.5 mg/kg, the same NP dose as that of in the NP- α -M) or α -M (1 mg/kg) or 0.9% saline was intravenously injected, respectively. After that, the mice were sacrificed and the brain slices were immunostained with anti-AT8 or anti-A β antibodies. Compared with other mice, NP- α -M treated mice had significantly reduced PHF and A β depositions in the cortex and hippocampus (Fig. 6A–F). But α -M did not develop the same effect

as NP- α -M (Fig. 6A–F), probably because its low bioavailability impeded its efficiency *in vivo*. These results indicated that NP- α -M promoted the clearance of misfolded proteins in the $3 \times$ TG mice. Misfolded proteins are regarded as a direct cause of synapse dysfunction and neuron death^{40–42}. Nissl staining showed that in the NP, α -M or saline treated mice, many neurons in the cortex and CA2 hippocampus were deeply stained, and had smaller and irregular shapes (Fig. 6G). But in the NP- α -M treated mice, most neurons remained light staining and round shape (Fig. 6G), which suggested that NP- α -M ameliorated the neuron damage in the $3 \times$ TG mice. The development of AD always accompanies with inflammation in the brain⁴³, so we measured some typical pro-inflammatory factors by ELISA, and found that NP- α -M reduced TNF- α , IL-1 β , and IL-6 levels both in the hippocampus and cortex (Fig. 6H). NP- α -M also rescued the learning and memory dysfunctions in the AD model mice. In the open field test (OFT), the moving distance and time of the NP- α -M treated mice and the saline treated mice had no difference (Supporting Information Figs. S11A–C), indicating that NP- α -M did not induce psychostimulant disturbances in the mice. In the object recognition test (ORT), compared with saline treated mice, NP- α -M treated mice exhibited more exploring interest on the new objects either in the short-time or long-time test (Fig. 6I), indicating that NP- α -M treatment meliorated the short-term and long-term memory of the $3 \times$ TG mice. In the Y-maze test, the percentage of the spontaneous alternation of the $3 \times$ TG mice was elevated upon NP- α -M treatment (Fig. 6J). In

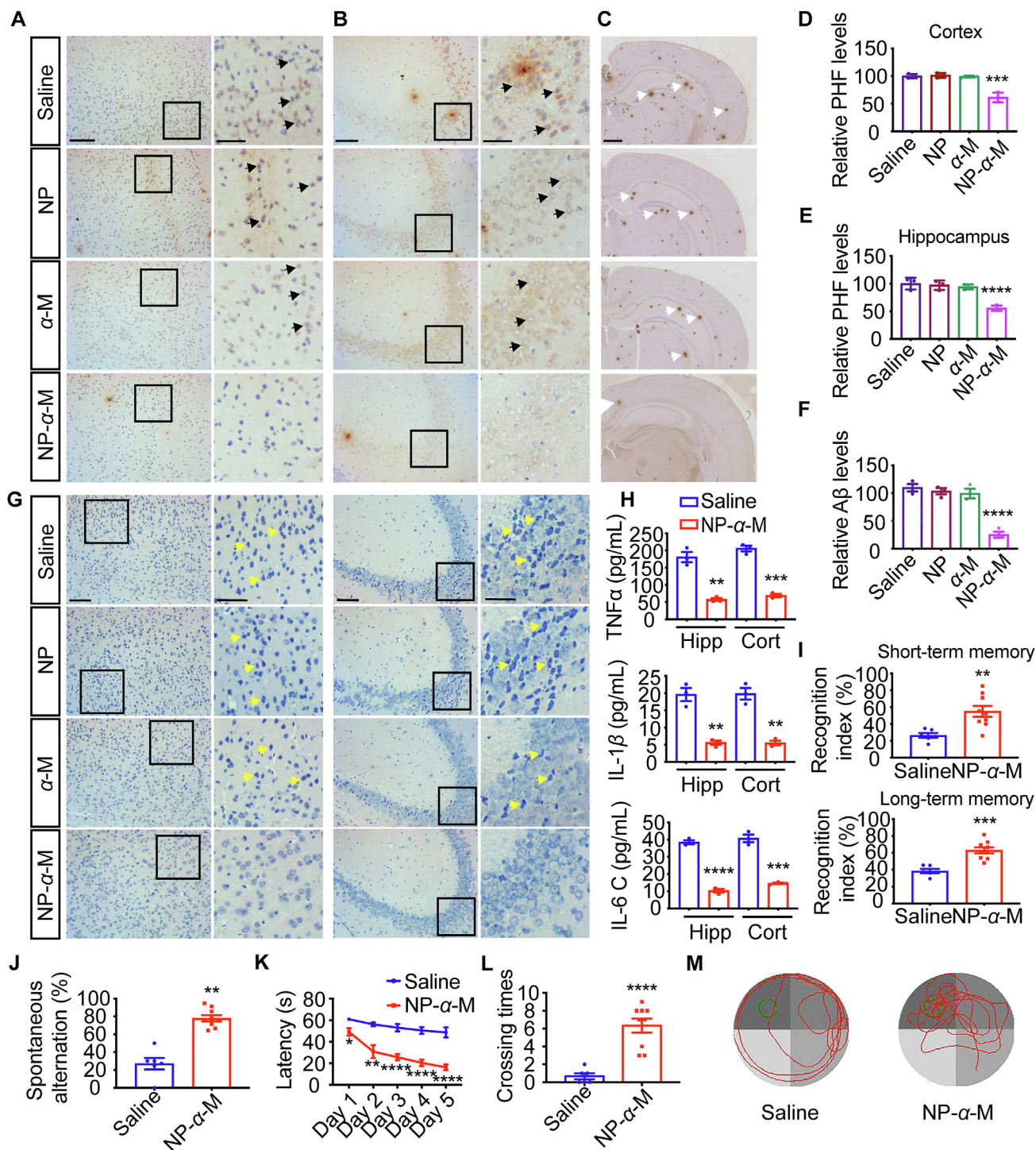


Figure 6 NP- α -M promotes A β and PHF clearance and rescues the neuropathology in AD model mice. 10-month-old 3 \times TG mice were intravenously injected with 0.9% saline, NP (the same NP dose as that of in the NP- α -M), α -M (1 mg/kg) or NP- α -M (α -M, 1 mg/kg) per day for one month. (A and B) Representative images of PHF (AT8) staining in the cortex (A) and hippocampus (B) from the 3 \times TG mice. Black arrows highlight PHF in the zoom-in areas enlarged from the boxes. Scale bar, 100 μ m. Zoom-in areas, scale bar, 50 μ m; (C) Representative images of A β (6E10) staining in the cortex and hippocampus from the 3 \times TG mice. White arrows highlight A β plaque. Scale bar, 500 μ m; (D to F) Quantification of PHF in the cortex (D), PHF in the hippocampus (E), and A β in the cortex and hippocampus (F) from the 3 \times TG mice using ImageJ software ($n = 3$ mice per group); (G) Representative images of Nissl staining in the cortex (left) and hippocampus (right) from the 3 \times TG mice. Scale bar, 100 μ m. Zoom-in areas were enlarged from the boxes, scale bar, 50 μ m; (H) The levels of pro-inflammatory cytokines including TNF- α , IL-1 β , and IL-6 in the cortex or hippocampus from the 3 \times TG mice treated with saline or NP- α -M were measured using ELISA kits ($n = 3$ mice per group). Hipp, Hippocampus. Cort, Cortex; (I) The recognition index in the object recognition test (ORT) ($n = 6-9$ mice per group); (J) The spontaneous alternation % in the Y-maze test ($n = 6-9$ mice per group); (K) Escape latency to the platform in the Morris' water

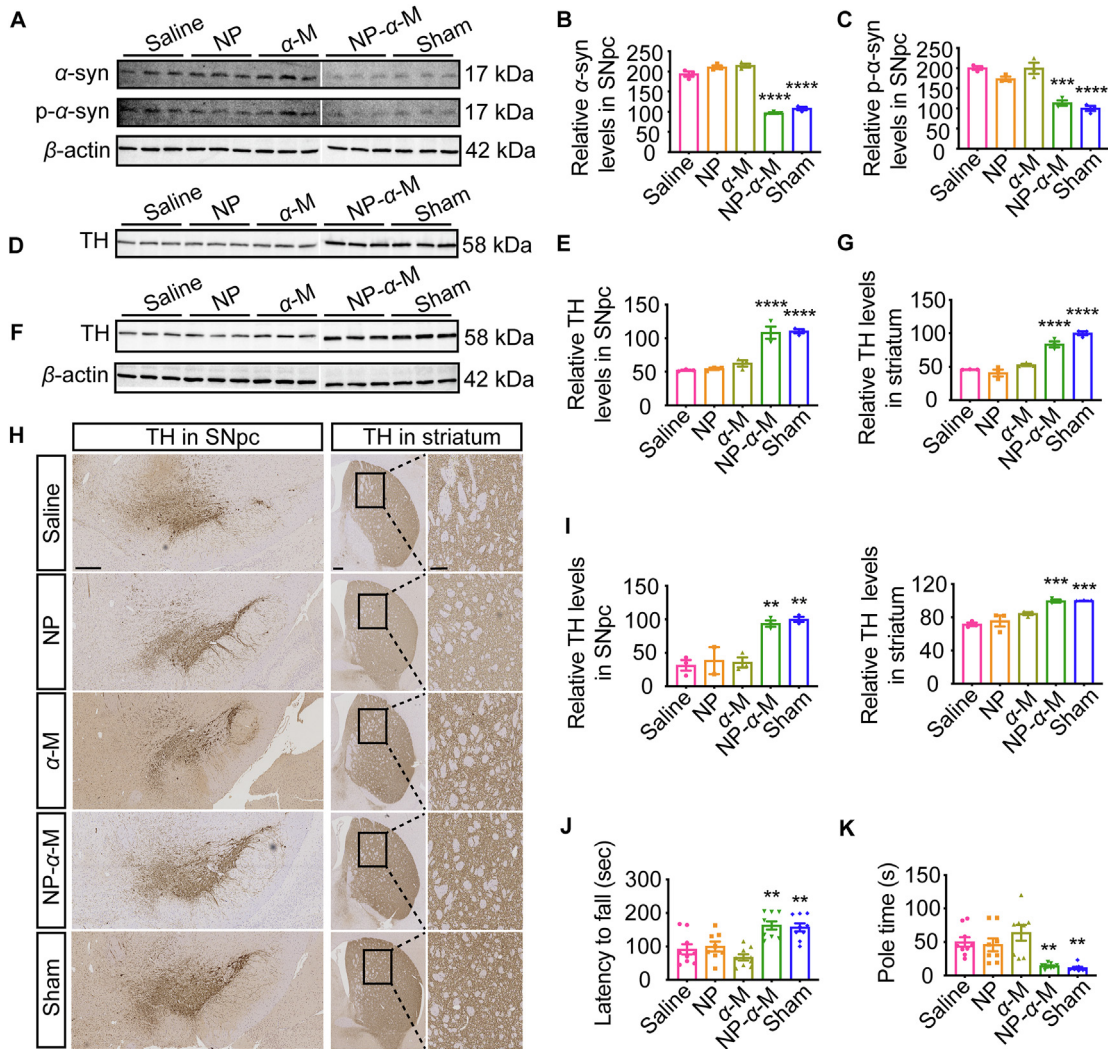


Figure 7 NP- α -M promotes PFF clearance and rescues the neuropathology in PD model mice. PD pathology was induced by PFF in C57BL/6 mice, and then the mice were intravenously injected with 0.9% saline, NP (the same NP dose as that of in the NP- α -M), α -M (1 mg/kg) or NP- α -M (α -M, 1 mg/kg) per day for one month. C57BL/6 mice without PFF-induced pathology but sham-operated were treated with 0.9% saline. (A to G) α -synuclein (α -syn), *p*- α -synuclein (*p*- α -syn) (A) and TH (D) were extracted from SNpc, and TH were extracted from the striatum (F), and examined by Western blot. The Lines' intensity was quantified using ImageJ software ($n = 3$ mice per group). The β -actin of TH in (A) is also the internal reference in (D). There is a white vertical line separated between α -M and NP- α -M in (A, D, and F), which means the lines of Saline, NP, α -M and the lines of NP- α -M, Sham are from two different gels. But the two gels were parallel conducted and then captured at the same time and place so as to maintain the comparability of the two gels; (H) Representative images of TH staining in the SNpc (left) and striatum (right) from the PD model mice. Scale bar, 500 μ m (SNpc), 100 μ m (striatum). Zoom-in areas were enlarged from the boxes, scale bar 50 μ m; (I) Quantification of TH in the SNpc and striatum from the PD model mice using ImageJ software ($n = 3$ mice per group, expect for the NP group in (i)); (J) The falling latency in the Rotarod test ($n = 8-9$ mice per group); (K) The climbing time to the bottom of the pole in the Pole test ($n = 8-9$ mice per group). Expression level was relative to the Sham group (B, C, E, G and I). Data are means \pm SEM. ** $P < 0.01$, *** $P < 0.001$, **** $P < 0.0001$ significantly different with that of the Saline group. One-way ANOVA, followed by Tukey's multiple comparisons test.

the Morris water maze test, NP- α -M treated mice had a shorter escape latency in the first 5 training days (Fig. 6K), and exhibited more crossing times (Fig. 6L), longer searching time and distance in the platform quadrant compared with saline treated mice in the following probe test (Fig. 6M and Figs. S11D

and E). The swimming speed among the mice showed no difference (Fig. S11F), suggesting that the speed did not interfere the results. Y-maze test and Morris water maze test collectively indicated that NP- α -M alleviated the learning and spatial memory defects in the 3 \times TG mice.

maze test ($n = 6-9$ mice per group); (L) Platform crossing times in the probe test ($n = 6-9$ mice per group); (M) Representative track images of the 3 \times TG mice in the probe test ($n = 6-9$ mice per group). Expression level was relative to the Saline group (D, E and F). Data are means \pm SEM. * $P < 0.05$, ** $P < 0.01$, *** $P < 0.001$, **** $P < 0.0001$ significantly different with that of the Saline group. Student's *t* test (H, I, J, K and L). One-way ANOVA (D, E, and F), followed by Tukey's multiple comparisons test.

3.6. NP- α -M promoted PFF clearance and relieved neuropathological changes in PD model mice

To measure the pathological changes in the PD model mice upon NP- α -M treatment, we first established the PD model mice, and after that we intravenously injected saline, NP, α -M or NP- α -M to the PD model mice (any dose in these treatments is the same as that of in the treatment of $3 \times$ TG mice). The sham operated mice were treated with 0.9% saline. We found that compared with saline, NP, α -M treated PD model mice, the levels of Triton X-100 insoluble α -synuclein (α -syn) and phosphorylated α -synuclein at Ser129 (p- α -syn) in the SNpc is significantly lower in NP- α -M treated PD model mice (Fig. 7A–C), indicating that NP- α -M promoted the clearance of misfolded proteins in the PD model mice. In dopaminergic neurons, tyrosine hydroxylase (TH) is the rate-limiting enzyme in the synthesis of DA⁴⁴. To evaluate the state of dopaminergic neurons, we detected TH in the SNpc and striatum by Western blot. We found that compared with sham-operated mice, TH levels in the striatum and SNpc of the saline, NP or α -M treated PD model mice were much lower (Fig. 7D–G). But in the NP- α -M treated PD model mice, TH was nearly the same level as that of in the sham-operated mice (Fig. 7D–G). Besides, brain sections of SNpc and striatum were immunostained with anti-TH antibody, and presented a similar outcome as Western blot (Fig. 7H and I). These results indicated that NP- α -M ameliorated the dysfunction of dopaminergic neurons in the PD model mice. The amelioration of dopaminergic neuron damage also rescued the motor deficits in the PD model mice. In the accelerating rotarod test, sham-operated mice or NP- α -M treated PD model mice spent more time on the moving rotarod than saline, NP or α -M treated PD model mice (Fig. 7J). In the pole test, sham-operated mice or NP- α -M treated PD model mice climbed much quicker from the top to the bottom of the pole than saline, NP or α -M treated PD model mice (Fig. 7K).

4. Discussion

Misfolded proteins, a hallmark of neurodegenerative diseases, play a key role in the pathogenesis of most neurodegenerative diseases¹. Therefore, clearing the misfolded proteins would be of great help to treat neurodegenerative diseases. At present, the eliminating strategy for the misfolded proteins include preventing the formation of the misfolded proteins or targeting the intracellular/extracellular clearance pathway was clarified³. But as multiple types of misfolded protein with different characteristics might together cause the disease and the uncertainties about which process or protein in the clearance pathway to target, making such strategy not efficient enough in practice³. Therefore, a more effective and universal approach to clear the misfolded proteins is still in urgent need.

Microglia is the resident macrophage in the CNS. As an innate function, microglia recognize the toxic substances include the misfolded proteins and safely clear them, which plays an essential role in maintaining brain homeostasis⁴. But in neurodegenerative diseases, a metabolic failure occurs and damages the surveillance function in microglia^{5,6,9,10}. Thus, restoring metabolic balance might be a promising strategy to recover microglial surveillance of the misfolded proteins. Present researches discovered that some drugs may relief the overactivation or inflammatory response of microglia by regulating metabolism⁶, but an effective metabolic modulator that is capable to rejuvenate microglial surveillance function in the diseases remains unavailable.

To find such modulator, we noticed that natural polyphenols such as resveratrol, quercetin and curcumin have been reported to intervene in metabolism-associated diseases including obesity¹² and diabetes¹¹. Therefore, we proposed that polyphenols might be potential metabolic modulators for the dysfunctional microglia in neurodegenerative diseases. Our previous study found that a natural polyphenol, α -M, promoted microglial clearance of A β in AD¹³, so we presumed that α -M might be able to rejuvenate microglial surveillance of misfolded proteins through metabolic modulation and serve as a universal therapy against various neurodegenerative diseases.

To verify the above hypothesis, we performed RNAseq and found that α -M/NP- α -M reprogrammed metabolism in microglia, and OXPHOS in glucose metabolism was majorly enhanced. As a metabolic switch from OXPHOS to glycolysis occurred in microglia in neurodegeneration⁶, α -M/NP- α -M might be able to rescue such metabolic failure in microglia. So, we used Seahorse to verify the change of glucose metabolism and found that diseased-associated microglia underwent an energy-shortage dilemma manifested by a switch from OXPHOS to glycolysis, but α -M/NP- α -M shifted the glycolysis back to OXPHOS and recovered the sufficient energy supply in microglia. Collectively, RNAseq and Seahorse together indicated that α -M/NP- α -M reprogrammed metabolism which induced a metabolic shift from glycolysis to OXPHOS in diseased-associated microglia to restore the energy balance. As the survive and function of microglia crucially rely on the sufficient energy supply, the recovery of metabolic balance might be a salvation for microglial function, and thus enhanced the surveillance of misfolded proteins in neurodegeneration.

Though polyphenols possess many beneficial bioactivities, their application was strictly limited due to their low dietary intake, vulnerability to environmental variables, poor bioavailability and low permeability across the blood brain barrier (BBB)^{45–47}. Increasing the amount of free α -M may enhance effectiveness, but may also result in severe toxicity^{48,49}. Nanoformulations, including poly (ethylene glycol)-poly(L-lactide) (PEG–PLA) nanoparticles, have been successfully designed to overcome the limitations of polyphenols^{47,50–54}, holding potential to penetrate BBB in neurodegenerative diseases such as AD and PD^{55–57}. Furthermore, our recent study discovered that NP- α -M achieved BBB-crossing and microglia-targeting properties owing to the protein corona formed on the surface of the nanoparticle⁵⁸, and here we confirmed that NP- α -M did enhance α -M delivery into the microglia (Supporting Information Fig. S10). In the meanwhile, we discovered that NP- α -M exerted the same effect through the identical mechanism of action as free α -M, while blank nanoparticle (NP) hardly exerted any biological effect. These data collectively demonstrated nanotechnology as a promising technique for enabling the *in vivo* application of α -M, which would considerably expediting its clinical translation for the treatment of neurodegenerative diseases.

α -M reprogrammed the metabolism indicating that the molecular that conducted such broad effect might be a central metabolic controller in the cells. AMPK, a highly conserved intracellular kinase, is the principal sensor of cellular energy and the central regulator of cellular metabolism in the cell upon energetic stress conditions³³. AMPK activates when senses the decrease of cellular ATP, and then coordinates many types of metabolic pathway to inhibit ATP-consuming activities while enhancing ATP-generating activities, which resulting in a holistic recovery of energy balance³³. AMPK regulates metabolism holistically³³, and also increases ATP and recovers energy balance like that of upon α -M/

NP- α -M treatment, so we presumed that α -M/NP- α -M might regulate metabolism through AMPK in microglia. To verify this hypothesis, we measured the Thr172 phosphorylation of α -subunit in AMPK and related Ser428 phosphorylation of LKB1 and expression of PGC-1 α . Thr172 phosphorylation of the α -subunit in AMPK is the main event in the full activation of AMPK³³, while the main kinase to phosphorylate Thr172 in AMPK is LKB1, which through the phosphorylation at Ser428^{59–61}. One of the important downstream transcriptional regulator of AMPK is PGC-1 α , which regulates mitochondrial biogenesis and respiration⁶². By detecting these key molecules, we disclosed that AMPK activation was essential for α -M/NP- α -M recovered metabolic balance in diseased-associated microglia.

Next, we investigated whether α -M/NP- α -M could rejuvenate microglial surveillance of misfolded proteins through the AMPK-mediated metabolic recovery. Microglial surveillance clears the misfolded proteins through phagocytosis and degradation^{63–66}. Here we discovered that inhibiting AMPK abolished α -M/NP- α -M enhancing microglial clearance of PFF and PHF (Fig. 3D and F), suggesting that AMPK is critical in α -M/NP- α -M function. Interestingly, we also found that although α -M and NP- α -M achieved the similar level of AMPK activation in the diseased-associated microglia (Fig. 2A–C), NP- α -M-treated microglia phagocytized and degraded more misfolded proteins than α -M-treated microglia (Fig. 3C and E). Such findings suggested that a more sophisticated mechanism might also be involved in the function of NP- α -M. Our previous study found that NP- α -M promoted the phagocytosis of nanoparticle⁶⁷, which could lead to increased internalization of α -M and empower NP- α -M a more powerful effect than free α -M. In addition, LC3-associated phagocytosis (LAP), which promotes both phagocytosis and degradation⁶⁸, may also play a role in the function of α -M/NP- α -M.

Phagocytosis is an energy-intensive process^{6,34}, it explained AMPK-mediated metabolic recovery by α -M/NP- α -M promoted the phagocytosis of misfolded proteins. But we also found that AMPK was essential for promoting microglial degradation of the misfolded proteins. As degradation is an energy-producing process that does not require as much energy as phagocytosis³⁵, so it is not clear that why α -M/NP- α -M also promoted the degradation of the misfolded proteins through AMPK-mediated metabolic restoration. Autophagy, a common cellular process, associates with both degradation and metabolism. Autophagy is a major way for microglia to degrade phagocytosed-particles³⁶, and it is also an energy-producing process³⁷, therefore it is possible that α -M/NP- α -M restored the metabolic balance through autophagy while autophagy increased the degradation of the misfolded proteins. To verify this hypothesis, we evaluated autophagy activity and disclosed that α -M/NP- α -M enhanced autophagy to degrade the misfolded proteins. But how AMPK involved in needed further investigation. Like AMPK, mTOR plays a vital role in regulating metabolism and connects with AMPK³⁸, but mTOR is also a crucial regulator in autophagy³⁹. So, we presumed that α -M/NP- α -M might enhance autophagy through AMPK-mTOR pathway in microglia. We found that α -M/NP- α -M indeed inhibited mTOR and thus induced autophagy in microglia, and the inhibition of mTOR relied on AMPK activation. Collectively, we demonstrated that α -M/NP- α -M enhanced autophagy for restoring metabolic balance which also rejuvenated microglial degradation of the misfolded proteins. In the investigation process, we also observed an interesting phenomenon that either the inhibition of mTOR or up-regulation of LC3-II by α -M/NP- α -M was blocked by compound C in the presence of the misfolded proteins (Fig. 5A–D),

but was not affected by compound C when misfolded proteins were absence (Figs. S8A–D). These results suggested that α -M/NP- α -M without misfolded proteins did not need AMPK to induce autophagy, but such autophagy is much weaker than AMPK-involved autophagy. As shown in Fig. 4A, the average LC3-II expression after α -M/NP- α -M treatment was about 1.6 times of the untreated control, but in Fig. 5A and D that the average LC3-II expression in the α -M/NP- α -M and misfolded proteins treatment was about 4.8 times of the untreated control. Though AMPK-involved autophagy is much stronger, that was not harmful to the cell, as shown in Fig. 1C–G and Figs. S2C–E that the AMPK-involved autophagy did not aggravate but rescued the dysfunctional metabolism in microglia. As for how microglia deployed AMPK to induce autophagy upon α -M/NP- α -M and misfolded proteins treatment, we speculated that was because α -M/NP- α -M reversed the damaged activation state of AMPK upon misfolded proteins treatment and thus making AMPK active to induce autophagy.

Despite that α -M/NP- α -M significantly modulated AMPK activation to regulate metabolism and clearance function in microglia, whether other cell type in the brain such as astrocyte involved in α -M/NP- α -M function is not clear. But as astrocytic clearance is a compensatory mechanism when microglial clearance is impaired⁶⁹, and NP- α -M primarily accumulated in microglia in the brain (Fig. S10), microglia remained the major cell type in NP- α -M function. Besides, whether AMPK is the direct target of α -M/NP- α -M remained unclear. Future work to explore the exact target molecular of α -M/NP- α -M would be important to fully understand the mechanism and provide novel drug targets for holistically promoting the surveillance function in microglia.

5. Conclusions

Collectively, we demonstrated that α -M/NP- α -M reprogrammed the metabolism and restored the metabolic balance by inducing a shift from glycolysis to OXPHOS in disease-associated microglia, which holistically rejuvenated microglial surveillance of the misfolded proteins. Our study provided a novel method for clearing misfolded proteins through reprogramming metabolism in microglia and demonstrated that NP- α -M might be a universal drug to treat various neurodegenerative diseases.

Acknowledgments

This work was supported by National Natural Science Foundation of China (Nos. 81722043, 92068111, 81973272, 82073836, 81903582, China), and granted from Shanghai Science and Technology Committee (19410710100; 121XD1422200, China).

Author contributions

Xiaoling Gao and Hongzhan Chen conceived the project. Dayuan Wang designed and conducted the experiments. The entire project was supervised by Xiaoling Gao and Hongzhan Chen. Xiao Gu, Xinyi Ma, Jun Chen, Qizhi Zhang, Zhihua Yu, Juan Li, Meng Hu, Xiaofang Tan, Yuyun Tang, Jianrong Xu, Minjun Xu, Qingxiang Song, Huahua Song, Gan Jiang and Zaiming Tang provided some essential materials and technique supports. Dayuan Wang, Xiaoling Gao and Hongzhan Chen wrote the manuscript. All of the authors have read and approved the final manuscript.

Conflicts of interest

The authors declare no conflicts of interest.

Appendix A. Supporting information

Supporting data to this article can be found online at <https://doi.org/10.1016/j.apsb.2022.07.014>.

References

- Soto C, Pritzkow S. Protein misfolding, aggregation, and conformational strains in neurodegenerative diseases. *Nat Neurosci* 2018;**21**:1332–40.
- Jucker M, Walker LC. Propagation and spread of pathogenic protein assemblies in neurodegenerative diseases. *Nat Neurosci* 2018;**21**:1341–9.
- Sweeney P, Park H, Baumann M, Dunlop J, Frydman J, Kopito R, et al. Protein misfolding in neurodegenerative diseases: implications and strategies. *Transl Neurodegener* 2017;**6**:6.
- Colonna M, Butovsky O. Microglia function in the central nervous system during health and neurodegeneration. *Annu Rev Immunol* 2017;**35**:441–68.
- Hickman S, Izzy S, Sen P, Morsett L, El Khoury J. Microglia in neurodegeneration. *Nat Neurosci* 2018;**21**:1359–69.
- Aldana BI. Microglia-specific metabolic changes in neurodegeneration. *J Mol Biol* 2019;**431**:1830–42.
- Baik SH, Kang S, Lee W, Choi H, Chung S, Kim JI, et al. A breakdown in metabolic reprogramming causes microglia dysfunction in Alzheimer's Disease. *Cell Metab* 2019;**30**:493–507. e6.
- Monzio Compagnoni G, Di Fonzo A, Corti S, Comi GP, Bresolin N, Masliah E. The role of mitochondria in neurodegenerative diseases: the lesson from Alzheimer's disease and Parkinson's disease. *Mol Neurobiol* 2020;**57**:2959–80.
- Asai H, Ikezu S, Tsunoda S, Medalla M, Luebke J, Haydar T, et al. Depletion of microglia and inhibition of exosome synthesis halt tau propagation. *Nat Neurosci* 2015;**18**:1584–93.
- Lee DC, Rizer J, Selenica ML, Reid P, Kraft C, Johnson A, et al. LPS-induced inflammation exacerbates phospho-tau pathology in rTg4510 mice. *J Neuroinflammation* 2010;**7**:56.
- Quero J, Marmol I, Cerrada E, Rodrıguez-Yoldi MJ. Insight into the potential application of polyphenol-rich dietary intervention in degenerative disease management. *Food Funct* 2020;**11**:2805–25.
- Boccellino M, D'Angelo S. Anti-obesity effects of polyphenol intake: current status and future possibilities. *Int J Mol Sci* 2020;**21**.
- Yao L, Gu X, Song QX, Wang XL, Huang M, Hu M, et al. Nano-formulated alpha-mangostin ameliorates Alzheimer's disease neuropathology by elevating LDLR expression and accelerating amyloid-beta clearance. *J Control Release* 2016;**226**:1–14.
- Song QX, Huang M, Yao L, Wang XL, Gu X, Chen J, et al. Lipoprotein-based nanoparticles rescue the memory loss of mice with Alzheimer's disease by accelerating the clearance of amyloid-beta. *ACS Nano* 2014;**8**:2345–59.
- Gao XL, Wu BX, Zhang QZ, Chen J, Zhu JH, Zhang WW, et al. Brain delivery of vasoactive intestinal peptide enhanced with the nanoparticles conjugated with wheat germ agglutinin following intranasal administration. *J Control Release* 2007;**121**:156–67.
- Yun SP, Kam TI, Panicker N, Kim S, Oh Y, Park JS, et al. Block of A1 astrocyte conversion by microglia is neuroprotective in models of Parkinson's disease. *Nat Med* 2018;**24**:931–8.
- Ait-Bouziad N, Lv G, Mahul-Mellier AL, Xiao SF, Zorludemir G, Eliezer D, et al. Discovery and characterization of stable and toxic tau/phospholipid oligomeric complexes. *Nat Commun* 2017;**8**:1678.
- Goedert M, Jakes R, Spillantini MG, Hasegawa M, Smith MJ, Crowther RA. Assembly of microtubule-associated protein tau into Alzheimer-like filaments induced by sulphated glycosaminoglycans. *Nature* 1996;**383**:550–3.
- Majerova P, Zilkova M, Kazmerova Z, Kovac A, Paholikova K, Kovacech B, et al. Microglia display modest phagocytic capacity for extracellular tau oligomers. *J Neuroinflammation* 2014;**11**:161.
- Lee HJ, Suk JE, Bae EJ, Lee SJ. Clearance and deposition of extracellular alpha-synuclein aggregates in microglia. *Biochem Biophys Res Commun* 2008;**372**:423–8.
- Luo WJ, Liu WC, Hu XY, Hanna M, Caravaca A, Paul SM. Microglial internalization and degradation of pathological tau is enhanced by an anti-tau monoclonal antibody. *Sci Rep* 2015;**5**:11161.
- Fronza MG, Baldinotti R, Martins MC, Goldani B, Dalberto BT, Kremer FS, et al. Rational design, cognition and neuropathology evaluation of QTC-4-MeOBnE in a streptozotocin-induced mouse model of sporadic Alzheimer's disease. *Sci Rep* 2019;**9**:7276.
- Vorhees CV, Williams MT. Morris water maze: procedures for assessing spatial and related forms of learning and memory. *Nat Protoc* 2006;**1**:848–58.
- Feldman AT, Wolfe D. Tissue processing and hematoxylin and eosin staining. *Methods Mol Biol* 2014;**1180**:31–43.
- Lee Y, Karuppagounder SS, Shin JH, Lee YI, Ko HS, Swing D, et al. Parthanatos mediates AIMP2-activated age-dependent dopaminergic neuronal loss. *Nat Neurosci* 2013;**16**:1392–400.
- He ZH, Guo JL, McBride JD, Narasimhan S, Kim H, Changolkar L, et al. Amyloid-beta plaques enhance Alzheimer's brain tau-seeded pathologies by facilitating neuritic plaque tau aggregation. *Nat Med* 2018;**24**:29–38.
- Wang ZY, Yuan BQ, Fu FL, Huang SK, Yang Z. Hemoglobin enhances miRNA-144 expression and autophagic activation mediated inflammation of microglia via mTOR pathway. *Sci Rep* 2017;**7**:11861.
- Choi SY, Lopez-Gonzalez R, Krishnan G, Phillips HL, Li AN, Seeley WW, et al. C9ORF72-ALS/FTD-associated poly(GR) binds Atp5a1 and compromises mitochondrial function *in vivo*. *Nat Neurosci* 2019;**22**:851–62.
- Wang MX, Cheng XY, Jin M, Cao YL, Yang YP, Wang JD, et al. TNF compromises lysosome acidification and reduces alpha-synuclein degradation via autophagy in dopaminergic cells. *Exp Neurol* 2015;**271**:112–21.
- Kim JD, Yoon NA, Jin S, Diano S. Microglial UCP2 mediates inflammation and obesity induced by high-fat feeding. *Cell Metab* 2019;**30**:952–62. e5.
- Bonora M, Patergnani S, Rimessi A, De Marchi E, Suski JM, Bononi A, et al. ATP synthesis and storage. *Purinergic Signal* 2012;**8**:343–57.
- Singh A, Kukreti R, Saso L, Kukreti S. Oxidative stress: a key modulator in neurodegenerative diseases. *Molecules* 2019;**24**.
- Garcia D, Shaw RJ. AMPK: mechanisms of cellular energy sensing and restoration of metabolic balance. *Mol Cell* 2017;**66**:789–800.
- Engl E, Attwell D. Non-signalling energy use in the brain. *J Physiol* 2015;**593**:3417–29.
- Rabinowitz JD, White E. Autophagy and metabolism. *Science* 2010;**330**:1344–8.
- Glick D, Barth S, Macleod KF. Autophagy: cellular and molecular mechanisms. *J Pathol* 2010;**221**:3–12.
- Plaza-Zabala A, Sierra-Torre V, Sierra A. Autophagy and microglia: novel partners in neurodegeneration and aging. *Int J Mol Sci* 2017;**18**:598.
- Inoki K, Kim J, Guan KL. AMPK and mTOR in cellular energy homeostasis and drug targets. *Annu Rev Pharmacol Toxicol* 2012;**52**:381–400.
- Kim YC, Guan KL. mTOR: a pharmacologic target for autophagy regulation. *J Clin Invest* 2015;**125**:25–32.
- Viola KL, Klein WL. Amyloid β oligomers in Alzheimer's disease pathogenesis, treatment, and diagnosis. *Acta Neuropathol* 2015;**129**:183–206.
- Guo T, Noble W, Hanger DP. Roles of tau protein in health and disease. *Acta Neuropathol* 2017;**133**:665–704.
- Volpicelli-Daley LA, Luk KC, Patel TP, Tanik SA, Riddle DM, Stieber A, et al. Exogenous α -synuclein fibrils induce Lewy body pathology leading to synaptic dysfunction and neuron death. *Neuron* 2011;**72**:57–71.

43. Akiyama H, Barger S, Barnum S, Bradt B, Bauer J, Cole GM, et al. Inflammation and Alzheimer's disease. *Neurobiol Aging* 2000;**21**: 383–421.
44. Shehadeh J, Double KL, Murphy KE, Bobrovskaya L, Reyes S, Dunkley PR, et al. Expression of tyrosine hydroxylase isoforms and phosphorylation at serine 40 in the human nigrostriatal system in Parkinson's disease. *Neurobiol Dis* 2019;**130**:104524.
45. Pandit R, Chen L, Götz J. The blood-brain barrier: physiology and strategies for drug delivery. *Adv Drug Deliv Rev* 2020;**165–166**: 1–14.
46. Caruso G, Torrisi SA, Mogavero MP, Currenti W, Castellano S, Godos J, et al. Polyphenols and neuroprotection: therapeutic implications for cognitive decline. *Pharmacol Therapeut* 2022;**232**:108013.
47. Yang BY, Dong YX, Wang F, Zhang Y. Nanoformulations to enhance the bioavailability and physiological functions of polyphenols. *Molecules* 2020;**25**.
48. Kittipaspallop W, Taepavaraprak P, Chanchao C, Pimtong W. Acute toxicity and teratogenicity of α -mangostin in zebrafish embryos. *Exp Biol Med (Maywood)* 2018;**243**:1212–9.
49. Zhang KJ, Gu QL, Yang K, Ming XJ, Wang JX. Anticarcinogenic effects of α -mangostin: a review. *Planta Med* 2017;**83**:188–202.
50. Chen Y, Lu Y, Lee RJ, Xiang GY. Nano encapsulated curcumin: and its potential for biomedical applications. *Int J Nanomed* 2020;**15**: 3099–120.
51. Aiello P, Consalvi S, Poce G, Raguzzini A, Toti E, Palmery M, et al. Dietary flavonoids: nano delivery and nanoparticles for cancer therapy. *Semin Cancer Biol* 2021;**69**:150–65.
52. Hardy N, Viola H, Johnstone V, Clemons T, Cserne Szappanos H, Singh R, et al. Nanoparticle-mediated dual delivery of an antioxidant and a peptide against the L-type Ca^{2+} channel enables simultaneous reduction of cardiac ischemia-reperfusion injury. *ACS Nano* 2015;**9**:279–89.
53. Hendawy OM. Nano-delivery systems for improving therapeutic efficiency of dietary polyphenols. *Altern Ther Health Med* 2021;**27**: 162–77.
54. Squillaro T, Cimini A, Peluso G, Giordano A, Melone MAB. Nano-delivery systems for encapsulation of dietary polyphenols: an experimental approach for neurodegenerative diseases and brain tumors. *Biochem Pharmacol* 2018;**154**:303–17.
55. Khan NU, Ni J, Ju XF, Miao TT, Chen HY, Han L. Escape from abluminal LRP1-mediated clearance for boosted nanoparticle brain delivery and brain metastasis treatment. *Acta Pharm Sin B* 2021;**11**:1341–54.
56. Han L, Jiang C. Evolution of blood-brain barrier in brain diseases and related systemic nanoscale brain-targeting drug delivery strategies. *Acta Pharm Sin B* 2021;**11**:2306–25.
57. Li J, Sabliov C. PLA/PLGA nanoparticles for delivery of drugs across the blood–brain barrier. *Nanotechnol Rev* 2013;**2**:241–57.
58. Tang YL, Gao JC, Wang T, Zhang Q, Wang AT, Huang M, et al. The effect of drug loading and multiple administration on the protein corona formation and brain delivery property of PEG-PLA nanoparticles. *Acta Pharm Sin B* 2022;**12**:2043–56.
59. Alessi DR, Sakamoto K, Bayascas JR. LKB1-dependent signaling pathways. *Annu Rev Biochem* 2006;**75**:137–63.
60. Xie ZL, Dong YZ, Zhang M, Cui MZ, Cohen RA, Riek U, et al. Activation of protein kinase c zeta by peroxy nitrite regulates LKB1-dependent AMP-activated protein kinase in cultured endothelial cells. *J Biol Chem* 2006;**281**:6366–75.
61. Hou XY, Xu SQ, Maitland-Toolan KA, Sato K, Jiang BB, Ido Y, et al. SIRT1 regulates hepatocyte lipid metabolism through activating AMP-activated protein kinase. *J Biol Chem* 2008;**283**:20015–26.
62. Herzig S, Shaw RJ. AMPK: guardian of metabolism and mitochondrial homeostasis. *Nat Rev Mol Cell Biol* 2018;**19**:121–35.
63. Fu RY, Shen QY, Xu PF, Luo JJ, Tang YM. Phagocytosis of microglia in the central nervous system diseases. *Mol Neurobiol* 2014;**49**: 1422–34.
64. Berglund R, Guerreiro-Cacais AO, Adzemovic MZ, Zeitelhofer M, Lund H, Ewing E, et al. Microglial autophagy-associated phagocytosis is essential for recovery from neuroinflammation. *Sci Immunol* 2020;**5**.
65. Choi I, Zhang YX, Seegobin SP, Pruvost M, Wang Q, Purtell K, et al. Microglia clear neuron-released α -synuclein via selective autophagy and prevent neurodegeneration. *Nat Commun* 2020;**11**:1386.
66. Wu AG, Zhou XG, Qiao G, Yu L, Tang Y, Yan L, et al. Targeting microglial autophagic degradation in NLRP3 inflammasome-mediated neurodegenerative diseases. *Ageing Res Rev* 2021;**65**:101202.
67. Wang DY, Song HH, Hu M, Li J, Gu X, Gao XL. Comparison in effects of α M and NP- α M on microglial uptake of A β . *Shandong Med J* 2019;**59**:24–8.
68. Lai SC, Devenish RJ. LC3-associated phagocytosis (LAP): connections with host autophagy. *Cells* 2012;**1**:396–408.
69. Konishi H, Okamoto T, Hara Y, Komine O, Tamada H, Maeda M, et al. Astrocytic phagocytosis is a compensatory mechanism for microglial dysfunction. *The EMBO journal* 2020;**39**:e104464.